Embracing Nonlinearities in Future Wireless Communication Systems: Low-Resolution Analog-to-Digital Converters

Khodor Safa
Supervisors: Raul De Lacerda, Sheng Yang

Université Paris-Saclay, CNRS, CentraleSupélec, Laboratoire des Signaux et Systèmes, 91190, Gif-sur-Yvette, France.

25 November 2024

Jury Members

Philippe CIBLAT Professeur, Télécom Paris	Rapporteur & Examinateur
Inbar FIJALKOW Professeure, ENSEA, CNRS	Rapporteure & Examinatrice
Jean-Philippe OVARLEZ Directeur de Recherche, ONERA	Examinateur
Maxime GUILLAUD Directeur de Recherche, INRIA Lyon	Examinateur

Table of contents

Current Section

1. Introduction
2. System Model and Receiver Design
3. One-bit Data Detection with Perfect CSI
4. Data Detection with statistical CSI
5. Future Perspectives and Conclusions

Road towards future wireless systems

- Ever-increasing requirements on throughput, latency and reliability

Road towards future wireless systems

- Ever-increasing requirements on throughput, latency and reliability
- Emergence of new technologies

Road towards future wireless systems

- Ever-increasing requirements on throughput, latency and reliability
- Emergence of new technologies
- Increase in bandwidths and carrier frequencies

Road towards future wireless systems

- Ever-increasing requirements on throughput, latency and reliability
- Emergence of new technologies
- Increase in bandwidths and carrier frequencies

Accompanying challenges and limitations

- Stricter constraints on radio-frequency (RF) components design

Road towards future wireless systems

- Ever-increasing requirements on throughput, latency and reliability
- Emergence of new technologies
- Increase in bandwidths and carrier frequencies

Accompanying challenges and limitations

- Stricter constraints on radio-frequency (RF) components design
- Cost and energy efficiency

Road towards future wireless systems

- Ever-increasing requirements on throughput, latency and reliability
- Emergence of new technologies
- Increase in bandwidths and carrier frequencies

Accompanying challenges and limitations

- Stricter constraints on radio-frequency (RF) components design
- Cost and energy efficiency
- Nonlinear characteristics in, e.g., power amplifiers (PAs), local oscillators, and analog-to-digital converters (ADCs)

Road towards future wireless systems

- Ever-increasing requirements on throughput, latency and reliability
- Emergence of new technologies
- Increase in bandwidths and carrier frequencies

Accompanying challenges and limitations

- Stricter constraints on radio-frequency (RF) components design
- Cost and energy efficiency
- Nonlinear characteristics in, e.g., power amplifiers (PAs), local oscillators, and analog-to-digital converters (ADCs)

ADC impairments

- Aperture jitter in the sample-and-hold (SAH) circuitry

$$z(nT_s) = x(nT_s + \varepsilon(nT_s))$$

- Quantization distortion

$$y[n] = Q_b(z[n])$$

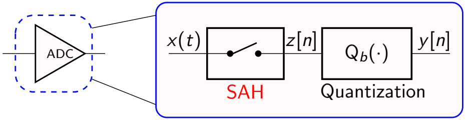

Figure: ADC functionality composed of a sampling circuitry then quantizing the output

ADC impairments

- Aperture jitter in the sample-and-hold (SAH) circuitry

$$z(nT_s) = x(nT_s + \varepsilon(nT_s))$$

- Quantization distortion

$$y[n] = Q_b(z[n])$$

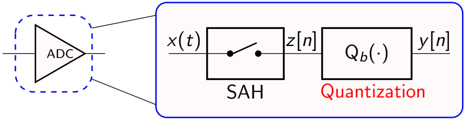

Figure: ADC functionality composed of a sampling circuitry then quantizing the output

ADC impairments

- Aperture jitter in the sample-and-hold (SAH) circuitry

$$z(nT_s) = x(nT_s + \varepsilon(nT_s))$$

- Quantization distortion

$$y[n] = Q_b(z[n])$$

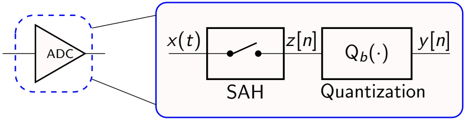

Figure: ADC functionality composed of a sampling circuitry then quantizing the output

What about power consumption?

- Energy efficiency
- It can become a bottleneck especially as system complexity increases
- How to characterize these criteria for ADCs?

Analog-to-digital Converters (1)

How to assess the technology trend of ADCs?

- ADCs can have different designs
- Quantifying their performance can be non-trivial

Analog-to-digital Converters (1)

How to assess the technology trend of ADCs?

- ADCs can have different designs
- Quantifying their performance can be non-trivial

$\rightarrow$ We consider figures of merit (FoMs)

Analog-to-digital Converters (1)

How to assess the technology trend of ADCs?

- ADCs can have different designs
- Quantifying their performance can be non-trivial

→ We consider figures of merit (FoMs)

ADC performance characterization

First notable survey in 1999 by Robert H. Walden [Wal99]

- FoM that relates power dissipation P to sampling frequency, f_s, and resolution b[1]

$$P = F_W \cdot f_s \cdot 2^b \tag{1}$$

[1] In practice, the resolution is usually measured as the effective number of bits (ENOB) also related to the signal-to-noise-distortion (SNDR) as ENOB = (SNDR − 1.62)/6.02

Analog-to-digital Converters (1)

How to assess the technology trend of ADCs?

- ADCs can have different designs
- Quantifying their performance can be non-trivial

$\rightarrow$ We consider figures of merit (FoMs)

ADC performance characterization

First notable survey in 1999 by Robert H. Walden [Wal99]

- FoM that relates power dissipation P to sampling frequency, f_s, and resolution b[1]

$$P = F_W \cdot f_s \cdot 2^b \tag{1}$$

- Aperture jitter limitation

[1] In practice, the resolution is usually measured as the effective number of bits (ENOB) also related to the signal-to-noise-distortion (SNDR) as ENOB = (SNDR − 1.62)/6.02

Analog-to-digital Converters (1)

How to assess the technology trend of ADCs?

- ADCs can have different designs
- Quantifying their performance can be non-trivial

$\rightarrow$ We consider figures of merit (FoMs)

ADC performance characterization

First notable survey in 1999 by Robert H. Walden [Wal99]

- FoM that relates power dissipation P to sampling frequency, f_s, and resolution b[1]

$$P = F_W \cdot f_s \cdot 2^b \tag{1}$$

- Aperture jitter limitation

Power scales linearly in the sampling frequency, and exponentially in the resolution.

[1] In practice, the resolution is usually measured as the effective number of bits (ENOB) also related to the signal-to-noise-distortion (SNDR) as ENOB $=$ (SNDR $-$ 1.62)/6.02

Recent surveys also show that [Bin+05; Mur15]

- Quadrupling in power as resolution increases

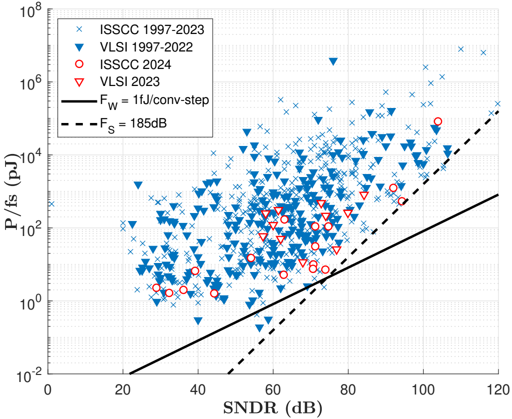

Figure: ADC energy performance survey data collected from IEEE ISSCC and VLSI Symposium .

Recent surveys also show that [Bin+05; Mur15]

- Quadrupling in power as resolution increases
- Schreir FoM

$$F_S = \mathrm{SNDR} + 10 \cdot \log\left(\frac{f_s}{2P}\right) \tag{2}$$

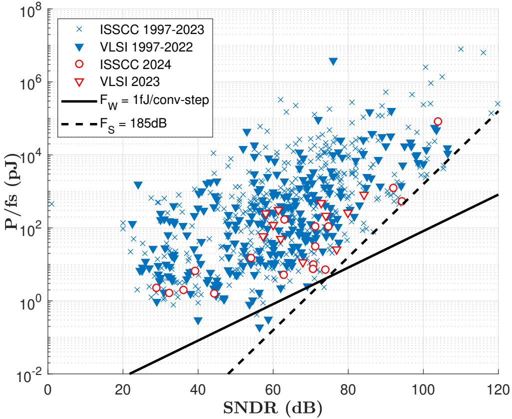

Figure: ADC energy performance survey data collected from IEEE ISSCC and VLSI Symposium .

Recent surveys also show that [Bin+05; Mur15]

- Quadrupling in power as resolution increases
- Schreir FoM

$$F_S = \text{SNDR} + 10 \cdot \log\left(\frac{f_s}{2P}\right) \quad (2)$$

- Aperture jitter remains a limiting factor

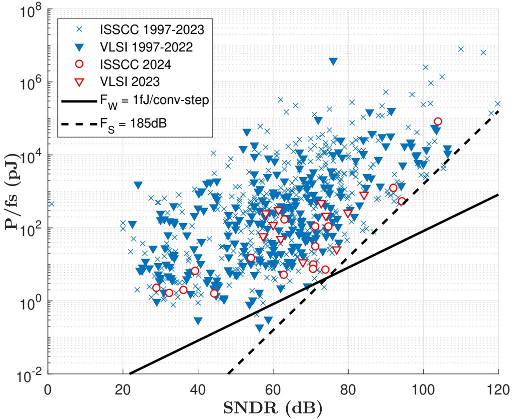

Figure: ADC energy performance survey data collected from IEEE ISSCC and VLSI Symposium .

Recent surveys also show that [Bin+05; Mur15]

- Quadrupling in power as resolution increases
- Schreir FoM

$$F_S = \text{SNDR} + 10 \cdot \log\left(\frac{f_s}{2P}\right) \quad (2)$$

- Aperture jitter remains a limiting factor

→ What if we employ low-resolution ADCs at the cost of more signal distortion?

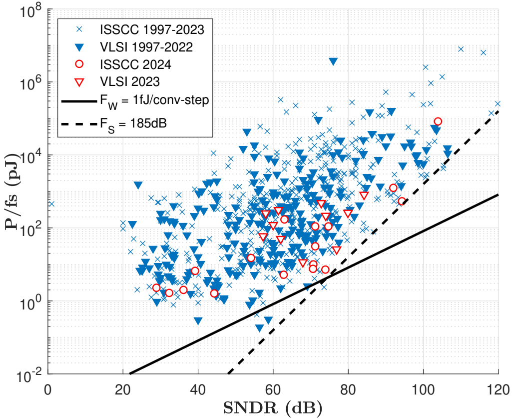

Figure: ADC energy performance survey data collected from IEEE ISSCC and VLSI Symposium .

Low-Resolution ADCs: Challenges

Employing low-resolution ADCs at the receiver can incur several challenges

Challenges

- Data detection
- Channel Estimation

Related work

For data detection and channel estimation

- Linear techniques and Nonlinear techniques [Jac+17; AT22; CMH16; NSN21a]

Low-Resolution ADCs: Challenges

Employing low-resolution ADCs at the receiver can incur several challenges

Challenges

- Data detection
- Channel Estimation
- Characterizing the capacity

Related work

For data detection and channel estimation

- Linear techniques and Nonlinear techniques [Jac+17; AT22; CMH16; NSN21a]
- SISO AWGN channel and MIMO fading channel in specific asymptotic regimes [SDM09; MNS20; YC24a]

Low-Resolution ADCs: Challenges

Employing low-resolution ADCs at the receiver can incur several challenges

Challenges

- Data detection
- Channel Estimation
- Characterizing the capacity
- Energy-spectral efficiency tradeoff

Related work

For data detection and channel estimation

- Linear techniques and Nonlinear techniques [Jac+17; AT22; CMH16; NSN21a]
- SISO AWGN channel and MIMO fading channel in specific asymptotic regimes [SDM09; MNS20; YC24a]
- Joint energy and rate assessments [QAN13; OER15; LR23]

Open Research Areas to Explore

Open areas

The maximum likelihood (ML) detection problem:

- With perfect channel state information at the receiver (CSIR), the complexity grows exponentially in the number of transmitters
- Without CSI, need to estimate the channel.

Understanding the energy-rate trade-off

- Requires characterizing the capacity
- The noncoherent setting remains not fully explored

Main Contributions and On-Going Work (1)

Main contributions

One-bit ML data detection problem with CSIR:

- Two-stage data detection algorithm that extends conventional sphere-decoding (SD) to the one-bit quantized channel

Main Contributions and On-Going Work (1)

Main contributions

One-bit ML data detection problem with CSIR:

- Two-stage data detection algorithm that extends conventional sphere-decoding (SD) to the one-bit quantized channel
- The approach is extended to the multi-bit case

Main Contributions and On-Going Work (1)

Main contributions

One-bit ML data detection problem with CSIR:

- Two-stage data detection algorithm that extends conventional sphere-decoding (SD) to the one-bit quantized channel
- The approach is extended to the multi-bit case

With only statistical CSI:

Main Contributions and On-Going Work (1)

Main contributions

One-bit ML data detection problem with CSIR:

- Two-stage data detection algorithm that extends conventional sphere-decoding (SD) to the one-bit quantized channel
- The approach is extended to the multi-bit case

With only statistical CSI:

- Binary classification problem using probit regression framework

Main Contributions and On-Going Work (1)

Main contributions

One-bit ML data detection problem with CSIR:

- Two-stage data detection algorithm that extends conventional sphere-decoding (SD) to the one-bit quantized channel
- The approach is extended to the multi-bit case

With only statistical CSI:

- Binary classification problem using probit regression framework
- For a real channel model, we propose a closed-form expression to the ML metric

Main Contributions and On-Going Work (2)

These contributions have also appeared in the following publications

Publications

- K. Safa, R. De Lacerda, and S. Yang, "Channel Estimation and Data Detection in MIMO channels with 1-bit ADC using Probit Regression," *2023 IEEE Information Theory Workshop (ITW)*.
- K. Safa, R. Combes, R. de Lacerda and S. Yang, "Data Detection in 1-bit Quantized MIMO Systems," *IEEE Transactions on Communications*, vol. 72, no. 9, pp. 5396-5410, Sept. 2024

On-going work

We take a first step into understanding rate-energy efficiency trade-off when employing low-resolution ADCs:

- We can apply the results of Clarke and Barron [CB94] when the number of receive antennas is large
- For the noncoherent channel, we look at the unquantized channel as an upperbound for specific choices of the coherence interval

Current Section

We consider a MIMO transmission model with M transmit and N receive antennas

$$\tilde{\boldsymbol{y}} = \tilde{\mathrm{Q}}_b(\tilde{\boldsymbol{H}}\tilde{\boldsymbol{x}} + \tilde{\boldsymbol{z}}), \tag{3}$$

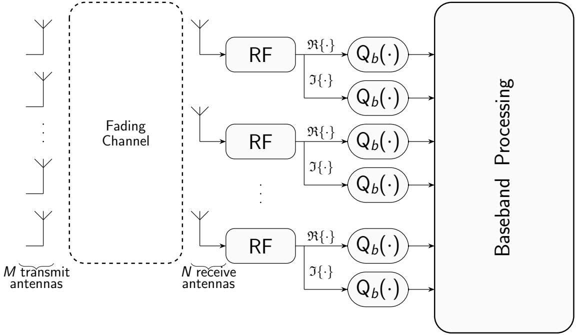

System Model (1)

We consider a MIMO transmission model with M transmit and N receive antennas

$$\tilde{\boldsymbol{y}} = \tilde{\mathrm{Q}}_b(\tilde{\boldsymbol{H}}\tilde{\boldsymbol{x}} + \tilde{\boldsymbol{z}}), \tag{3}$$

Where:

- **Transmitted signal**: $\tilde{\boldsymbol{x}} \in \tilde{\mathcal{X}}^M$, with $\tilde{\mathcal{X}}$ (e.g. QPSK, 16-QAM).

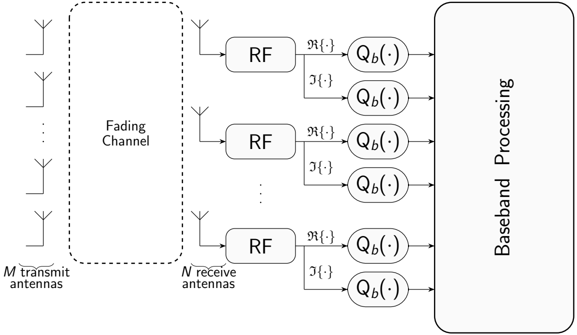

System Model (1)

We consider a MIMO transmission model with M transmit and N receive antennas

$$\tilde{\boldsymbol{y}} = \tilde{\mathrm{Q}}_b(\tilde{\boldsymbol{H}}\tilde{\boldsymbol{x}} + \tilde{\boldsymbol{z}}), \qquad (3)$$

- **Transmitted signal**: $\tilde{\boldsymbol{x}} \in \tilde{\mathcal{X}}^M$, with $\tilde{\mathcal{X}}$ (e.g. QPSK, 16-QAM).
- **Additive noise**: $\tilde{\boldsymbol{z}} \in \mathbb{C}^N$, $\tilde{z}_n \sim \mathcal{CN}(0, \tilde{\sigma}^2)$.

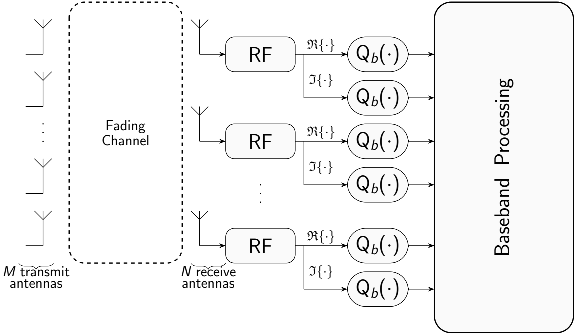

We consider a MIMO transmission model with M transmit and N receive antennas

$$\tilde{\boldsymbol{y}} = \tilde{\mathrm{Q}}_b(\tilde{\boldsymbol{H}}\tilde{\boldsymbol{x}} + \tilde{\boldsymbol{z}}), \tag{3}$$

- **Transmitted signal**: $\tilde{\boldsymbol{x}} \in \tilde{\mathcal{X}}^M$, with $\tilde{\mathcal{X}}$ (e.g. QPSK, 16-QAM).
- **Additive noise**: $\tilde{\boldsymbol{z}} \in \mathbb{C}^N$, $\tilde{z}_n \sim \mathcal{CN}(0, \tilde{\sigma}^2)$.
- **Channel matrix**: $\tilde{\boldsymbol{H}} \in \mathbb{C}^{N \times M}$, $\tilde{h}_{nm} \sim \mathcal{CN}(0, 1)$.

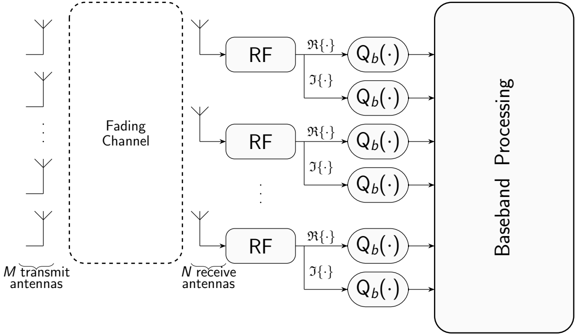

We consider a MIMO transmission model with M transmit and N receive antennas

$$\tilde{\boldsymbol{y}} = \tilde{\mathrm{Q}}_b(\tilde{\boldsymbol{H}}\tilde{\boldsymbol{x}} + \tilde{\boldsymbol{z}}), \tag{3}$$

- **Transmitted signal**: $\tilde{\boldsymbol{x}} \in \tilde{\mathcal{X}}^M$, with $\tilde{\mathcal{X}}$ (e.g. QPSK, 16-QAM).
- **Additive noise**: $\tilde{\boldsymbol{z}} \in \mathbb{C}^N$, $\tilde{z}_n \sim \mathcal{CN}(0, \tilde{\sigma}^2)$.
- **Channel matrix**: $\tilde{\boldsymbol{H}} \in \mathbb{C}^{N \times M}$, $\tilde{h}_{nm} \sim \mathcal{CN}(0, 1)$.
- **Quantizer**: A uniform midriser quantizer with resolution b and spacing δ

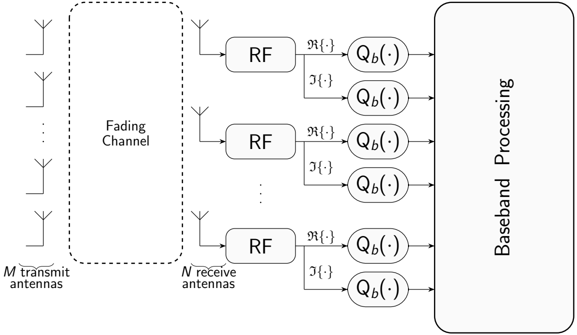

We consider a MIMO transmission model with M transmit and N receive antennas

$$\tilde{\boldsymbol{y}} = \tilde{\mathrm{Q}}_b(\tilde{\boldsymbol{H}}\tilde{\boldsymbol{x}} + \tilde{\boldsymbol{z}}), \qquad (3)$$

- **Transmitted signal**: $\tilde{\boldsymbol{x}} \in \tilde{\mathcal{X}}^M$, with $\tilde{\mathcal{X}}$ (e.g. QPSK, 16-QAM).
- **Additive noise**: $\tilde{\boldsymbol{z}} \in \mathbb{C}^N$, $\tilde{z}_n \sim \mathcal{CN}(0, \tilde{\sigma}^2)$.
- **Channel matrix**: $\tilde{\boldsymbol{H}} \in \mathbb{C}^{N\times M}$, $\tilde{h}_{nm} \sim \mathcal{CN}(0,1)$.
- **Quantizer**: A uniform midriser quantizer with resolution b and spacing δ
- **Quantized received signal**: $\tilde{\boldsymbol{y}} \in \tilde{\mathcal{Y}}_b^N$ a finite set of complex numbers.

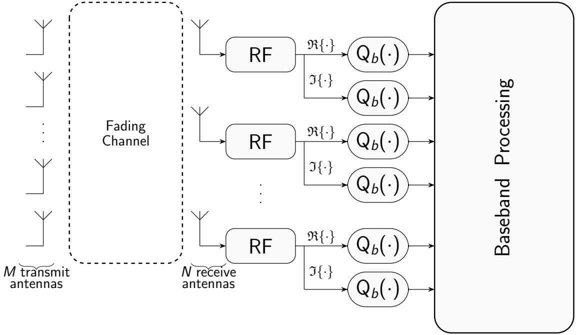

System Model (2)

We work with the real-equivalent channel model:

$$\begin{bmatrix} \Re\{\tilde{\boldsymbol{y}}\} \\ \Im\{\tilde{\boldsymbol{y}}\} \end{bmatrix} = \mathrm{Q}_b\left(\begin{bmatrix} \Re\{\tilde{\boldsymbol{H}}\} & -\Im\{\tilde{\boldsymbol{H}}\} \\ \Im\{\tilde{\boldsymbol{H}}\} & \Re\{\tilde{\boldsymbol{H}}\} \end{bmatrix} \begin{bmatrix} \Re\{\tilde{\boldsymbol{x}}\} \\ \Im\{\tilde{\boldsymbol{x}}\} \end{bmatrix} + \begin{bmatrix} \Re\{\tilde{\boldsymbol{z}}\} \\ \Im\{\tilde{\boldsymbol{z}}\} \end{bmatrix}\right),$$

$$\boldsymbol{y}_{2N} = \mathrm{Q}_b(\boldsymbol{H}_{2N \times 2M}\boldsymbol{x}_{2M} + \boldsymbol{z}_{2N}), \tag{4}$$

We work with the real-equivalent channel model:

$$\begin{bmatrix}\Re\{\tilde{\boldsymbol{y}}\}\\ \Im\{\tilde{\boldsymbol{y}}\}\end{bmatrix} = \mathrm{Q}_b\left(\begin{bmatrix}\Re\{\tilde{\boldsymbol{H}}\} & -\Im\{\tilde{\boldsymbol{H}}\}\\ \Im\{\tilde{\boldsymbol{H}}\} & \Re\{\tilde{\boldsymbol{H}}\}\end{bmatrix}\begin{bmatrix}\Re\{\tilde{\boldsymbol{x}}\}\\ \Im\{\tilde{\boldsymbol{x}}\}\end{bmatrix} + \begin{bmatrix}\Re\{\tilde{\boldsymbol{z}}\}\\ \Im\{\tilde{\boldsymbol{z}}\}\end{bmatrix}\right),$$
$$\boldsymbol{y}_{2N} = \mathrm{Q}_b(\boldsymbol{H}_{2N\times 2M}\boldsymbol{x}_{2M} + \boldsymbol{z}_{2N}), \tag{4}$$

$$\tilde{\mathrm{Q}}_b = \mathrm{Q}_b(\tilde{r}) + j\mathrm{Q}_b(\tilde{r}) \tag{5}$$

with $\mathrm{Q}_b(\cdot)$:

- Mapping from $\mathbb{R}$ to $\mathcal{Y}_b = \{\nu_1, \ldots, \nu_l, \ldots, \nu_{2^b}\}$
- $\mathcal{I} = \{\mathcal{I}_1, \ldots, \mathcal{I}_l, \ldots, \mathcal{I}_{2^b}\}$ where $\mathcal{I}_l = (l_{l-1}, l_l]$ and $l_l - l_{l-1} = \delta$

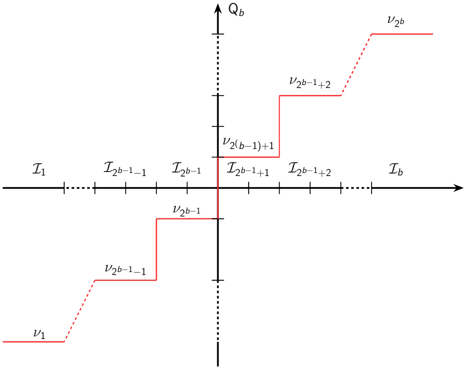

Figure: Characteristic of a uniform midriser quantizer with resolution b.

We work with the real-equivalent channel model:

$$\begin{bmatrix} \Re\{\tilde{\mathbf{y}}\} \\ \Im\{\tilde{\mathbf{y}}\} \end{bmatrix} = \mathrm{Q}_b\left(\begin{bmatrix} \Re\{\tilde{\boldsymbol{H}}\} & -\Im\{\tilde{\boldsymbol{H}}\} \\ \Im\{\tilde{\boldsymbol{H}}\} & \Re\{\tilde{\boldsymbol{H}}\} \end{bmatrix} \begin{bmatrix} \Re\{\tilde{\mathbf{x}}\} \\ \Im\{\tilde{\mathbf{x}}\} \end{bmatrix} + \begin{bmatrix} \Re\{\tilde{\mathbf{z}}\} \\ \Im\{\tilde{\mathbf{z}}\} \end{bmatrix} \right),$$

$$\mathbf{y}_{2N} = \mathrm{Q}_b(\boldsymbol{H}_{2N\times 2M}\mathbf{x}_{2M} + \mathbf{z}_{2N}), \tag{4}$$

$$\tilde{\mathrm{Q}}_b = \mathrm{Q}_b(\tilde{r}) + j\mathrm{Q}_b(\tilde{r}) \tag{5}$$

with $\mathrm{Q}_b(\cdot)$:

- Mapping from $\mathbb{R}$ to $\mathcal{Y}_b = \{\nu_1, \ldots, \nu_l, \ldots, \nu_{2^b}\}$
- $\mathcal{I} = \{\mathcal{I}_1, \ldots, \mathcal{I}_l, \ldots, \mathcal{I}_{2^b}\}$ where $\mathcal{I}_l = (I_{l-1}, I_l]$ and $I_l - I_{l-1} = \delta$

When $b = 1$ $\tilde{\mathrm{Q}}_1(\tilde{r}) = \mathrm{sgn}(\Re\{\tilde{r}\}) + j\mathrm{sgn}(\Im\{\tilde{r}\})$

$$\mathrm{sgn}(a) = \begin{cases} 1, & a \geq 0 \\ -1, & a < 0 \end{cases} \tag{6}$$

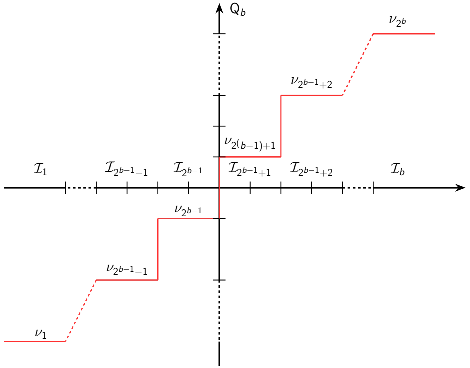

Figure: Characteristic of a uniform midriser quantizer with resolution b.

Optimization approach using the statistical structure of the model

Channel likelihood with receiver CSI

Map each element $\boldsymbol{y}_n$ to its associated index for the corresponding interval, i.e., from $y_n \in \mathcal{Y}_b$ to $\mathrm{y}_n \in \{1, 2, \ldots, l, \ldots, 2^b\}$:

$$\begin{aligned}\boldsymbol{P}(\boldsymbol{y}|\boldsymbol{x}, \boldsymbol{H}) &= \prod_{n=1}^{2N} \boldsymbol{P}(r_n \in \mathcal{I}_{\mathrm{y}_n}|\boldsymbol{h}_n, \boldsymbol{x}) \\ &= \prod_{n=1}^{2N} \left[\Phi\left(\frac{l_{\mathrm{y}_n} - \boldsymbol{h}_n^{\mathsf{T}}\boldsymbol{x}}{\sigma}\right) - \Phi\left(\frac{l_{\mathrm{y}_n-1} - \boldsymbol{h}_n^{\mathsf{T}}\boldsymbol{x}}{\sigma}\right)\right].\end{aligned} \tag{7}$$

$$\begin{aligned}\boldsymbol{x}^* &= \underset{\boldsymbol{x}\in\mathcal{X}^{2M}}{\arg\min} \; -\ln\left[\boldsymbol{P}(\boldsymbol{y}|\boldsymbol{H}, \boldsymbol{x})\right] \\ &= \underset{\boldsymbol{x}\in\mathcal{X}^{2M}}{\arg\min} \; -\sum_{n=1}^{2N} \ln\left[\Phi\left(\frac{l_{\mathrm{y}_n} - \boldsymbol{h}_n^{\mathsf{T}}\boldsymbol{x}}{\sigma}\right) - \Phi\left(\frac{l_{\mathrm{y}_n-1} - \boldsymbol{h}_n^{\mathsf{T}}\boldsymbol{x}}{\sigma}\right)\right] \\ &= \underset{\boldsymbol{x}\in\mathcal{X}^{2M}}{\arg\min} \; \ell_b(\boldsymbol{x}).\end{aligned} \tag{8}$$

Receiver Design (3)

Optimization approach using the statistical structure of the model

Channel likelihood with receiver CSI

Map each element $\boldsymbol{y}_n$ to its associated index for the corresponding interval, i.e., from $y_n \in \mathcal{Y}_b$ to $\mathrm{y}_n \in \{1, 2, \ldots, l, \ldots, 2^b\}$:

$$\boldsymbol{P}(\boldsymbol{y}|\boldsymbol{x}, \boldsymbol{H}) = \prod_{n=1}^{2N} \boldsymbol{P}(r_n \in \mathcal{I}_{\mathrm{y}_n} | \boldsymbol{h}_n, \boldsymbol{x})$$
$$= \prod_{n=1}^{2N} \left[\Phi\left(\frac{l_{\mathrm{y}_n} - \boldsymbol{h}_n^{\mathsf{T}} \boldsymbol{x}}{\sigma} \right) - \Phi\left(\frac{l_{\mathrm{y}_n - 1} - \boldsymbol{h}_n^{\mathsf{T}} \boldsymbol{x}}{\sigma} \right) \right]. \tag{7}$$

$$\begin{aligned} \boldsymbol{x}^* &= \underset{\boldsymbol{x} \in \mathcal{X}^{2M}}{\arg\min} \; -\ln\left[\boldsymbol{P}(\boldsymbol{y}|\boldsymbol{H}, \boldsymbol{x})\right] \\ &= \underset{\boldsymbol{x} \in \mathcal{X}^{2M}}{\arg\min} \; -\sum_{n=1}^{2N} \ln \left[\Phi\left(\frac{l_{\mathrm{y}_n} - \boldsymbol{h}_n^{\mathsf{T}} \boldsymbol{x}}{\sigma} \right) - \Phi\left(\frac{l_{\mathrm{y}_n - 1} - \boldsymbol{h}_n^{\mathsf{T}} \boldsymbol{x}}{\sigma} \right) \right] \\ &= \underset{\boldsymbol{x} \in \mathcal{X}^{2M}}{\arg\min} \; \ell_b(\boldsymbol{x}). \end{aligned} \tag{8}$$

Related work:

- Near Maximum Likelihood twos-tage approach [CMH16]
- One-bit sphere-decoding approach in [Jeo+18]
- Machine learning methods: SVM and deep learning approaches [NSN21b; Jeo+22; Kho+21]

Receiver Design (4)

Channel likelihood with only statistical CSI

Assuming a pilot training scheme

$$\left[\tilde{\boldsymbol{Y}}_p \ \tilde{\boldsymbol{Y}}_d\right] = \tilde{\mathrm{Q}}_b\left(\tilde{\boldsymbol{H}}\left[\tilde{\boldsymbol{X}}_p \ \tilde{\boldsymbol{X}}_d\right] + \left[\tilde{\boldsymbol{Z}}_p \ \tilde{\boldsymbol{Z}}_d\right]\right). \quad (9)$$

1. Obtain a point estimate

$$\hat{\boldsymbol{H}} = f(\tilde{\boldsymbol{X}}_p, \tilde{\boldsymbol{Y}}_p) \quad (10)$$

2. Evaluate the mismatched metric:

$$\boldsymbol{x}^* = \underset{\boldsymbol{x}\in\mathcal{X}^{2M}}{\arg\min} \ -\ln\left[\boldsymbol{P}\left(\boldsymbol{y}|\hat{\boldsymbol{H}}, \boldsymbol{x}\right)\right] \quad (11)$$

Related work:

- Multi-bit quantized a posteriori channel estimation for OFDM channels [SD16]
- Bayes-optimal joint channel and data detection using generalized approximate message passing (GAMP) [Wen+16]
- Deep learning methods using the deep unfolding technique [NSN21a; Kho+21]

Current Section

One-bit ML Data Detection with Perfect CSI

In the case where $b = 1$, the ML data detection problem becomes

$$\begin{aligned} \boldsymbol{x}_{\mathrm{ML}} &= \underset{\boldsymbol{x}\in\mathcal{X}^{2M}}{\arg\min} \quad -\sum_{n=1}^{2N} \ln\left[\Phi\left(\frac{y_n \boldsymbol{h}_n^{\mathsf{T}} \boldsymbol{x}}{\sigma}\right)\right] \\ &= \underset{\boldsymbol{x}\in\mathcal{X}^{2M}}{\arg\min} \quad \ell(\boldsymbol{x}). \end{aligned} \tag{12}$$

Main observations

- Combinatorial problem with search space of size $|\mathcal{X}|^{2M}$

One-bit ML Data Detection with Perfect CSI

In the case where $b = 1$, the ML data detection problem becomes

$$\begin{aligned} \boldsymbol{x}_{\mathrm{ML}} &= \underset{\boldsymbol{x} \in \mathcal{X}^{2M}}{\arg\min} \quad -\sum_{n=1}^{2N} \ln\left[\Phi\left(\frac{y_n \boldsymbol{h}_n^{\mathrm{T}} \boldsymbol{x}}{\sigma}\right)\right] \\ &= \underset{\boldsymbol{x} \in \mathcal{X}^{2M}}{\arg\min} \quad \ell(\boldsymbol{x}). \end{aligned} \tag{12}$$

Main observations

- Combinatorial problem with search space of size $|\mathcal{X}|^{2M}$
- Search space can be relaxed to $\mathbb{R}^{2M}$

One-bit ML Data Detection with Perfect CSI

In the case where $b = 1$, the ML data detection problem becomes

$$\begin{aligned} \boldsymbol{x}_{\mathrm{ML}} &= \underset{\boldsymbol{x}\in\mathcal{X}^{2M}}{\arg\min} \quad -\sum_{n=1}^{2N} \ln\left[\Phi\left(\frac{y_n \boldsymbol{h}_n^{\mathsf{T}}\boldsymbol{x}}{\sigma}\right)\right] \\ &= \underset{\boldsymbol{x}\in\mathcal{X}^{2M}}{\arg\min} \quad \ell(\boldsymbol{x}). \end{aligned} \tag{12}$$

Main observations

- Combinatorial problem with search space of size $|\mathcal{X}|^{2M}$
- Search space can be relaxed to $\mathbb{R}^{2M}$
- Objective function is concave

One-bit ML Data Detection with Perfect CSI

In the case where $b = 1$, the ML data detection problem becomes

$$\begin{aligned} \boldsymbol{x}_{\mathrm{ML}} &= \underset{\boldsymbol{x} \in \mathcal{X}^{2M}}{\arg\min} \quad -\sum_{n=1}^{2N} \ln \left[\Phi \left(\frac{y_n \boldsymbol{h}_n^{\mathrm{T}} \boldsymbol{x}}{\sigma} \right) \right] \\ &= \underset{\boldsymbol{x} \in \mathcal{X}^{2M}}{\arg\min} \quad \ell(\boldsymbol{x}). \end{aligned} \tag{12}$$

Main observations

- Combinatorial problem with search space of size $|\mathcal{X}|^{2M}$
- Search space can be relaxed to $\mathbb{R}^{2M}$
- Objective function is concave
- Rounding the result can be suboptimal

One-bit ML Data Detection with Perfect CSI

In the case where $b = 1$, the ML data detection problem becomes

$$\begin{aligned} \boldsymbol{x}_{\mathrm{ML}} &= \underset{\boldsymbol{x} \in \mathcal{X}^{2M}}{\arg\min} \quad -\sum_{n=1}^{2N} \ln \left[\Phi \left(\frac{y_n \boldsymbol{h}_n^{\mathrm{T}} \boldsymbol{x}}{\sigma} \right) \right] \\ &= \underset{\boldsymbol{x} \in \mathcal{X}^{2M}}{\arg\min} \quad \ell(\boldsymbol{x}). \end{aligned} \tag{12}$$

Main observations

- Combinatorial problem with search space of size $|\mathcal{X}|^{2M}$
- Search space can be relaxed to $\mathbb{R}^{2M}$
- Objective function is concave
- Rounding the result can be suboptimal

$\rightarrow$ Sphere-decoding can be used in the unquantized case, how to extend it for quantized observations?

Overview of proposed approach

1. Obtain initial estimate $\hat{\boldsymbol{x}}$ by relaxing discrete constraint

$$\boldsymbol{x}_{t+1} = \boldsymbol{x}_t - \zeta \nabla_{\ell(\boldsymbol{x}_t)}. \tag{13}$$

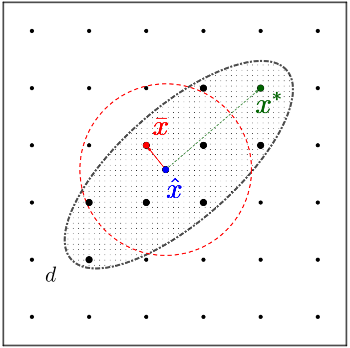

Figure: Illustration of one-bit SD in 2D.

One-Bit Sphere-Decoding (1)

Overview of proposed approach

1. Obtain initial estimate $\hat{\mathbf{x}}$ by relaxing discrete constraint

$$\mathbf{x}_{t+1} = \mathbf{x}_t - \zeta \nabla_{\ell(\mathbf{x}_t)}. \tag{13}$$

2. Approximate the likelihood around this point

$$\ell(\mathbf{x}) \approx \ell(\hat{\mathbf{x}}) + \frac{1}{2}(\mathbf{x} - \hat{\mathbf{x}})^T \nabla^2_{\ell(\hat{\mathbf{x}})} (\mathbf{x} - \hat{\mathbf{x}}) \tag{14}$$

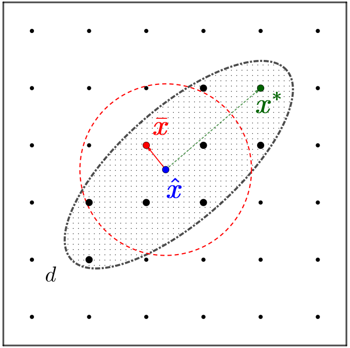

Figure: Illustration of one-bit SD in 2D.

One-Bit Sphere-Decoding (1)

Overview of proposed approach

1. Obtain initial estimate $\hat{\boldsymbol{x}}$ by relaxing discrete constraint

$$\boldsymbol{x}_{t+1} = \boldsymbol{x}_t - \zeta \nabla_{\ell(\boldsymbol{x}_t)}. \tag{13}$$

2. Approximate the likelihood around this point

$$\ell(\boldsymbol{x}) \approx \ell(\hat{\boldsymbol{x}}) + \frac{1}{2}(\boldsymbol{x} - \hat{\boldsymbol{x}})^T \nabla^2_{\ell(\hat{\boldsymbol{x}})}(\boldsymbol{x} - \hat{\boldsymbol{x}}) \tag{14}$$

3. Define a level set d

$$(\boldsymbol{x} - \hat{\boldsymbol{x}})^T \nabla^2_{\ell(\hat{\boldsymbol{x}})}(\boldsymbol{x} - \hat{\boldsymbol{x}}) = d. \tag{15}$$

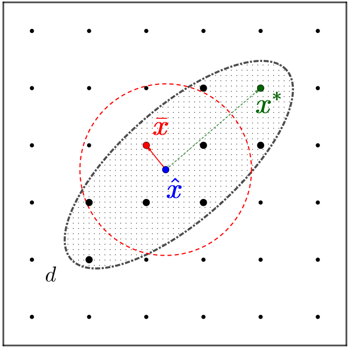

Figure: Illustration of one-bit SD in 2D.

Overview of proposed approach

1. Obtain initial estimate $\hat{\mathbf{x}}$ by relaxing discrete constraint

$$\mathbf{x}_{t+1} = \mathbf{x}_t - \zeta \nabla_{\ell(\mathbf{x}_t)}. \tag{13}$$

2. Approximate the likelihood around this point

$$\ell(\mathbf{x}) \approx \ell(\hat{\mathbf{x}}) + \frac{1}{2}(\mathbf{x} - \hat{\mathbf{x}})^T \nabla^2_{\ell(\hat{\mathbf{x}})} (\mathbf{x} - \hat{\mathbf{x}}) \tag{14}$$

3. Define a level set d

$$(\mathbf{x} - \hat{\mathbf{x}})^{\mathsf{T}} \nabla^2_{\ell(\hat{\mathbf{x}})} (\mathbf{x} - \hat{\mathbf{x}}) = d. \tag{15}$$

4. Perform a Cholesky decomposition $\nabla^2_{\ell(\hat{\mathbf{x}})} = \mathbf{R}^{\mathsf{T}}\mathbf{R}$

$$\begin{aligned} ||\mathbf{R}(\hat{\mathbf{x}} - \mathbf{x})||^2 &\leq d \\ ||\hat{\mathbf{t}} - \tilde{\mathbf{R}}\mathbf{s}||^2 &\leq d. \end{aligned} \tag{16}$$

where $\hat{\mathbf{t}} = \mathbf{R}(\hat{\mathbf{x}} - \mathbf{1}_{2M})$ and $\tilde{\mathbf{R}} = 2\mathbf{R}$

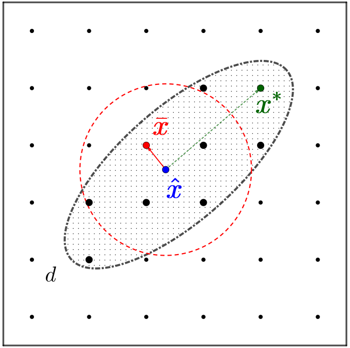

Figure: Illustration of one-bit SD in 2D.

Overview of proposed approach

5. each path at depth j has $\boldsymbol{s}_j^{2M} = [s_j, s_{j+1}, \ldots, s_{2M}]$ with weight

$$\varphi\left(\boldsymbol{s}_j^{2M}\right) = \sum_{i=j}^{2M} \left| \hat{t}_i - \sum_{m=i}^{2M} \tilde{r}_{i,m} s_m \right|^2 . \tag{17}$$

One-Bit Sphere-Decoding (2)

Overview of proposed approach

5. each path at depth j has $\boldsymbol{s}_j^{2M} = \left[s_j, s_{j+1}, \ldots, s_{2M}\right]$ with weight

$$\varphi\left(\boldsymbol{s}_j^{2M}\right) = \sum_{i=j}^{2M} \left| \hat{t}_i - \sum_{m=i}^{2M} \tilde{r}_{i,m} s_m \right|^2 . \tag{17}$$

6. Construct a tree with $2M$ levels where and enumerate all vectors such that

$$\varphi\left(\boldsymbol{s}_j^{2M}\right) \leq d, \qquad \text{for } j = [1, \ldots, 2M] . \tag{18}$$

Overview of proposed approach

5. each path at depth j has $\boldsymbol{s}_j^{2M} = \left[s_j, s_{j+1}, \ldots, s_{2M}\right]$ with weight

$$\varphi\left(\boldsymbol{s}_j^{2M}\right) = \sum_{i=j}^{2M} \left| \hat{t}_i - \sum_{m=i}^{2M} \tilde{r}_{i,m} s_m \right|^2 . \tag{17}$$

6. Construct a tree with $2M$ levels where and enumerate all vectors such that

$$\varphi\left(\boldsymbol{s}_j^{2M}\right) \leq d, \qquad \text{for } j = [1, \ldots, 2M] . \tag{18}$$

7. Fixing $|\mathcal{S}| = \tau$ during the enumeration. Output the τ closest vectors or leaf nodes

$$[\boldsymbol{s}_1, \ldots, \boldsymbol{s}_k, \ldots, \boldsymbol{s}_\tau] \tag{19}$$

sorted according to their weights

$$\boldsymbol{d} = [d_1, \ldots, d_k, \ldots, d_\tau], \tag{20}$$

where $d_k = \varphi(\boldsymbol{s}_k)$ and $d_1 \leq \ldots \leq d_k \leq \ldots \leq d_\tau$.

Overview of proposed approach

Define the following event

$$\mathcal{E} = \{\textit{The search sphere is not empty}\} \tag{21}$$

and set elements in $\boldsymbol{d}$ to ∞

Algorithm Sphere-decoding with one-bit ADCs

Input: $\boldsymbol{H}$, $\boldsymbol{y}$, σ, τ.
Initialization: Fix ζ, $t_{\max}$, ε, and $\boldsymbol{d}$ is set to ∞, $|\mathcal{S}| = \varnothing$.
Step 1: Obtain $\hat{\boldsymbol{x}}$ using gradient descent:
while $t \leq t_{\max}$ **and** $|\ell(\boldsymbol{x}_t) - \ell(\boldsymbol{x}_{t-1})| > \varepsilon|\ell(\boldsymbol{x}_{t-1})|$
    $\boldsymbol{x}_{t+1} = \boldsymbol{x}_t - \zeta\nabla_{\ell(\boldsymbol{x}_t)}$
end
Store $\hat{\boldsymbol{x}} = \boldsymbol{x}_{t_{\text{final}}}$.
Step 2: Cholesky factorization $\nabla^2_{\ell(\hat{\boldsymbol{x}})} = \boldsymbol{R}^{\mathsf{T}}\boldsymbol{R}$.
Step 3: Populate$\mathcal{S}$ algorithm and set $d = d_\tau$:
while $\mathcal{E}$ is true
    Find leaf node $\breve{\boldsymbol{x}}$ such that $\varphi(\breve{\boldsymbol{x}}) \leq d_\tau$
    Append $\mathcal{S} \leftarrow \breve{\boldsymbol{x}}$
    Update $\boldsymbol{d}(\tau) = \varphi(\breve{\boldsymbol{x}})$
    Sort $\boldsymbol{d}$ and $\mathcal{S}$ in ascending order of weights
    Update the sphere radius in $d = d_\tau$
end
Step 4: Find $\boldsymbol{x}^* = \arg\min_{\boldsymbol{x}\in\mathcal{S}} \ell(\boldsymbol{x})$.
Output: $\boldsymbol{x}_{\text{SD}} = \boldsymbol{x}^*$

One-Bit Sphere-Decoding (3)

Overview of proposed approach

Define the following event

$$\mathcal{E} = \{\textit{The search sphere is not empty}\} \tag{21}$$

and set elements in $\boldsymbol{d}$ to ∞

9. Translate back to constellation $\mathcal{X}$

$$\mathcal{S} = \left\{[\boldsymbol{x}_1, \ldots, \boldsymbol{x}_k, \ldots, \boldsymbol{x}_\tau] \in \mathcal{X}^{2M} \mid \|\boldsymbol{t} - \boldsymbol{R}\boldsymbol{x}_k\|^2 \leq d_\tau\right\}. \tag{22}$$

Algorithm Sphere-decoding with one-bit ADCs

Input: $\boldsymbol{H}$, $\boldsymbol{y}$, σ, τ.
Initialization: Fix ζ, $t_{\max}$, ε, and $\boldsymbol{d}$ is set to ∞, $|\mathcal{S}| = \varnothing$.
Step 1: Obtain $\hat{\boldsymbol{x}}$ using gradient descent:
while $t \leq t_{\max}$ **and** $|\ell(\boldsymbol{x}_t) - \ell(\boldsymbol{x}_{t-1})| > \varepsilon|\ell(\boldsymbol{x}_{t-1})|$
  $\boldsymbol{x}_{t+1} = \boldsymbol{x}_t - \zeta\nabla_{\ell(\boldsymbol{x}_t)}$
end
Store $\hat{\boldsymbol{x}} = \boldsymbol{x}_{t_{\text{final}}}$.
Step 2: Cholesky factorization $\nabla^2_{\ell(\hat{\boldsymbol{x}})} = \boldsymbol{R}^{\mathsf{T}}\boldsymbol{R}$.
Step 3: Populate $\mathcal{S}$ algorithm and set $d = d_\tau$:
while $\mathcal{E}$ is true
  Find leaf node $\breve{\boldsymbol{x}}$ such that $\varphi(\breve{\boldsymbol{x}}) \leq d_\tau$
  Append $\mathcal{S} \leftarrow \breve{\boldsymbol{x}}$
  Update $\boldsymbol{d}(\tau) = \varphi(\breve{\boldsymbol{x}})$
  Sort $\boldsymbol{d}$ and $\mathcal{S}$ in ascending order of weights
  Update the sphere radius in $d = d_\tau$
end
Step 4: Find $\boldsymbol{x}^* = \arg\min_{\boldsymbol{x}\in\mathcal{S}} \ell(\boldsymbol{x})$.
Output: $\boldsymbol{x}_{\text{SD}} = \boldsymbol{x}^*$

Overview of proposed approach

Define the following event

$$\mathcal{E} = \{\textit{The search sphere is not empty}\} \tag{21}$$

and set elements in $\boldsymbol{d}$ to ∞

9. Translate back to constellation $\mathcal{X}$

$$\mathcal{S} = \left\{[\boldsymbol{x}_1, \ldots, \boldsymbol{x}_k, \ldots, \boldsymbol{x}_\tau] \in \mathcal{X}^{2M} \mid ||\boldsymbol{t} - \boldsymbol{R}\boldsymbol{x}_k||^2 \leq d_\tau \right\}. \tag{22}$$

10. Evaluate likelihood over $\mathcal{S}$

$$\boldsymbol{x}_{\text{SD}} = \arg\min_{\boldsymbol{x} \in \mathcal{S}} \ \ell(\boldsymbol{x}). \tag{23}$$

Algorithm Sphere-decoding with one-bit ADCs

Input: $\boldsymbol{H}$, $\boldsymbol{y}$, σ, τ.
Initialization: Fix ζ, $t_{\max}$, ε, and $\boldsymbol{d}$ is set to ∞, $|\mathcal{S}| = \varnothing$.
Step 1: Obtain $\hat{\boldsymbol{x}}$ using gradient descent:
while $t \leq t_{\max}$ **and** $|\ell(\boldsymbol{x}_t) - \ell(\boldsymbol{x}_{t-1})| > \varepsilon|\ell(\boldsymbol{x}_{t-1})|$
    $\boldsymbol{x}_{t+1} = \boldsymbol{x}_t - \zeta\nabla_{\ell(\boldsymbol{x}_t)}$
end
Store $\hat{\boldsymbol{x}} = \boldsymbol{x}_{t_{\text{final}}}$.
Step 2: Cholesky factorization $\nabla^2_{\ell(\hat{\boldsymbol{x}})} = \boldsymbol{R}^{\mathsf{T}}\boldsymbol{R}$.
Step 3: Populate$\mathcal{S}$ algorithm and set $d = d_\tau$:
while $\mathcal{E}$ is true
    Find leaf node $\breve{\boldsymbol{x}}$ such that $\varphi(\breve{\boldsymbol{x}}) \leq d_\tau$
    Append $\mathcal{S} \leftarrow \breve{\boldsymbol{x}}$
    Update $\boldsymbol{d}(\tau) = \varphi(\breve{\boldsymbol{x}})$
    Sort $\boldsymbol{d}$ and $\mathcal{S}$ in ascending order of weights
    Update the sphere radius in $d = d_\tau$
end
Step 4: Find $\boldsymbol{x}^* = \arg\min_{\boldsymbol{x} \in \mathcal{S}} \ell(\boldsymbol{x})$.
Output: $\boldsymbol{x}_{\text{SD}} = \boldsymbol{x}^*$

Simulation Results (2)

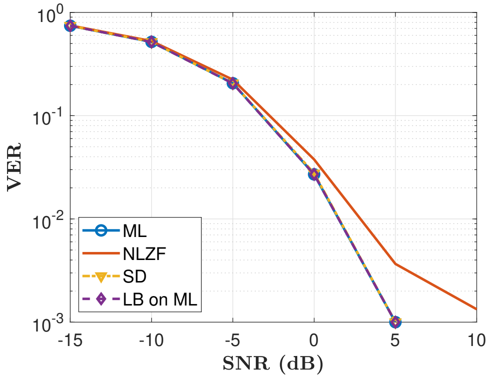

Figure: VER for 2×16-MIMO with QPSK, perfect CSI, and fixed candidates list cardinality $|\mathcal{S}| = 3$ for varying SNR.

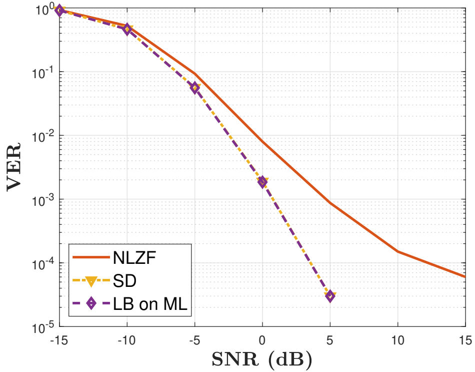

Figure: VER for 8×64-MIMO with QPSK, perfect CSI, and fixed candidates list cardinality $|\mathcal{S}| = 3$ for varying SNR.

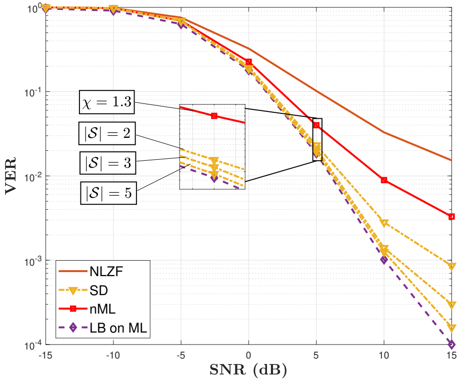

Figure: VER for 8 × 128-MIMO with 16-QAM, perfect CSI and varying SNR for several data detection metrics, and different sizes of $\mathcal{S}$.

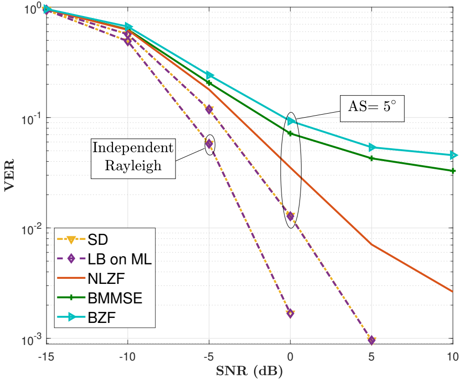

Figure: VER with QPSK, perfect CSI for a 10 × 72-MIMO system with one-bit quantization and a list size $|\mathcal{S}| = 5$. The angular spread for the correlated channels case is set to 5°.

Sphere-decoding for multi-bit ADCs with perfect CSI

Extension to multi-bit case

We can extend the previous work to the multi-bit case by obtaining the gradient and Hessian functions:

$$\nabla_{\ell_b(\mathbf{x})} = -\frac{1}{\sigma}\sum_{n=1}^{2N}\kappa_{b,\delta}\left(\frac{l_{y_n}-\mathbf{h}_n^{\mathrm{T}}\mathbf{x}}{\sigma},\frac{l_{y_n-1}-\mathbf{h}_n^{\mathrm{T}}\mathbf{x}}{\sigma}\right)\mathbf{h}_n \tag{24}$$

$$\nabla^2_{\ell_b(\mathbf{x})} = \frac{1}{\sigma^2}\sum_{n=1}^{2N}\eta_{b,\delta}\left(\frac{l_{y_n}-\mathbf{h}_n^{\mathrm{T}}\mathbf{x}}{\sigma},\frac{l_{y_n-1}-\mathbf{h}_n^{\mathrm{T}}\mathbf{x}}{\sigma}\right)\mathbf{h}_n\mathbf{h}_n^{\mathrm{T}} \tag{25}$$

with similar functions defined as

$$\kappa_{b,\delta}(u,v) = -\frac{\phi(u)-\phi(v)}{\Phi(u)-\Phi(v)}, \tag{26}$$

$$\eta_{b,\delta}(u,v) = \frac{u\phi(u)-v\phi(v)}{\Phi(u)-\Phi(v)} + \left(\kappa_{b,\delta}(u,v)\right)^2. \tag{27}$$

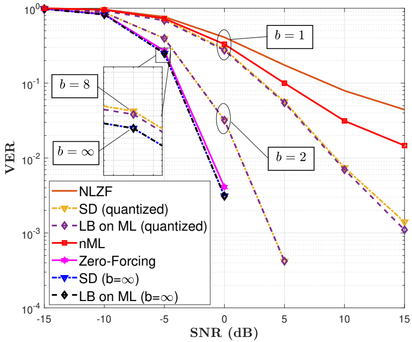

Figure: VER for 4 × 64-MIMO with 16-QAM, perfect CSI and varying SNR for several data detection metrics, and assumptions on the resolution b. The list size is fixed to $|\mathcal{S}| = 5$.

Current Section

Considering a pilot transmission scheme

- With a **pilot training scheme** such that $T = T_p + T_d$, we have:

$$[\tilde{\boldsymbol{Y}}_p \quad \tilde{\boldsymbol{Y}}_d] = \mathrm{Q}(\tilde{\boldsymbol{H}}\,[\tilde{\boldsymbol{X}}_{\boldsymbol{p}} \quad \tilde{\boldsymbol{X}}_{\boldsymbol{d}}] + [\tilde{\boldsymbol{Z}}_p \quad \tilde{\boldsymbol{Z}}_d]). \tag{28}$$

Key points:

- Present a two-step procedure for channel estimation and data detection in block-fading MIMO channels with 1-bit ADCs at the base station
- Investigate using this approach the instability reported in [NSN21b; NSN21a]
- Evaluate the performance with numerical simulations the SER and achievable mismatched rates based on the Generalized Mutual Information (GMI) for the different detection metrics
- We consider the optimal metric where channel estimation is conducted implicitly

Channel Estimation and Data Detection with Probit Regression (1)

Pilot transmission model:

$$\boldsymbol{Y}_p = \mathrm{Q}_1(\boldsymbol{X}_p\bar{\boldsymbol{H}} + \boldsymbol{Z}_p). \tag{29}$$

$$\begin{bmatrix} \Re\{\tilde{\boldsymbol{Y}}_p\}^\mathsf{T} \\ \Im\{\tilde{\boldsymbol{Y}}_p\}^\mathsf{T} \end{bmatrix} = \mathrm{Q}_b\left(\begin{bmatrix} \Re\{\tilde{\boldsymbol{X}}_p\} & \Im\{\tilde{\boldsymbol{X}}_p\} \\ -\Im\{\tilde{\boldsymbol{X}}_p\} & \Re\{\tilde{\boldsymbol{X}}_p\} \end{bmatrix}^\mathsf{T} \begin{bmatrix} \Re\{\tilde{\boldsymbol{H}}\}^\mathsf{T} \\ \Im\{\tilde{\boldsymbol{H}}\}^\mathsf{T} \end{bmatrix} + \begin{bmatrix} \Re\{\tilde{\boldsymbol{Z}}_p\}^\mathsf{T} \\ \Im\{\tilde{\boldsymbol{Z}}_p\}^\mathsf{T} \end{bmatrix} \right) \tag{30}$$

Channel estimation stage

Assuming a Gaussian prior on the channel vectors with i.i.d. elements, the MAP channel optimization problem can then be summarized as

$$\hat{\boldsymbol{h}}_n = \underset{\boldsymbol{h}_n \in \mathbb{R}^{2M}}{\arg\min}\; L_{\mathrm{CE}}(\bar{\boldsymbol{h}}_n) + \eta_p ||\bar{\boldsymbol{h}}_n||^2. \tag{31}$$

where

$$L_{\mathrm{CE}}(\bar{\boldsymbol{h}}_n) = -\frac{1}{2T_p} \sum_{t=1}^{2T_p} \left(\frac{y_{p,n}^t + 1}{2}\right) \ln\left[\Phi\left(\frac{\boldsymbol{h}_n^\mathsf{T} \boldsymbol{x}_{p,t}}{\sigma}\right)\right] + \left(\frac{1 - y_{p,n}^t}{2}\right) \ln\left[1 - \Phi\left(\frac{\boldsymbol{h}_n^\mathsf{T} \boldsymbol{x}_{p,t}}{\sigma}\right)\right] \tag{32}$$

Channel Estimation and Data Detection with Probit Regression (2)

Channel estimation stage

Let $\bar{\boldsymbol{\theta}}_n = \frac{\bar{\boldsymbol{h}}_n}{\sigma}$:

$$\hat{\boldsymbol{\theta}}_{n,k+1} = \hat{\boldsymbol{\theta}}_{n,k} - \zeta_p \nabla \mathcal{L}\left(\hat{\boldsymbol{\theta}}_n\right) \tag{33}$$

where

$$\nabla \mathcal{L}(\bar{\boldsymbol{\theta}}_n) = -\frac{1}{2T_p} \sum_{t=1}^{2T_p} \left[\frac{\frac{y_{p,n}^t + 1}{2} - \Phi\left(\bar{\boldsymbol{\theta}}_n^{\mathrm{T}} \boldsymbol{x}_{p,t}\right)}{\Phi\left(\bar{\boldsymbol{\theta}}_n^{\mathrm{T}} \boldsymbol{x}_{p,t}\right)\left(1 - \Phi\left(\bar{\boldsymbol{\theta}}_n^{\mathrm{T}} \boldsymbol{x}_{p,t}\right)\right)} \right] \times \left[\phi\left(\bar{\boldsymbol{\theta}}_n^{\mathrm{T}} \boldsymbol{x}_{p,t}\right)\right] + 2\eta_p \bar{\boldsymbol{\theta}}. \tag{34}$$

Form the estimated matrix

$$\hat{\boldsymbol{\Theta}} = \left[\hat{\boldsymbol{\theta}}_1, \ldots, \hat{\boldsymbol{\theta}}_n, \ldots, \hat{\boldsymbol{\theta}}_N\right] \tag{35}$$

Channel Estimation and Data Detection with Probit Regression (3)

Data transmission model:

$$\boldsymbol{Y}_d = \mathrm{Q}_1\left(\breve{\boldsymbol{H}}\boldsymbol{X}_d + \boldsymbol{Z}_d\right). \quad (36)$$

$$\begin{bmatrix} \Re\{\tilde{\boldsymbol{Y}}_d\} \\ \Im\{\tilde{\boldsymbol{Y}}_d\} \end{bmatrix} = \mathrm{Q}_1\left(\begin{bmatrix} \Re\{\tilde{\boldsymbol{H}}\} & -\Im\{\tilde{\boldsymbol{H}}\} \\ \Im\{\tilde{\boldsymbol{H}}\} & \Re\{\tilde{\boldsymbol{H}}\} \end{bmatrix} \begin{bmatrix} \Re\{\boldsymbol{X}_d\} \\ \Im\{\boldsymbol{X}_d\} \end{bmatrix} + \begin{bmatrix} \Re\{\boldsymbol{Z}_d\} \\ \Im\{\boldsymbol{Z}_d\} \end{bmatrix} \right). \quad (37)$$

Data detection stage

Assuming a box constraint, we obtain Under the hard box constraint, we obtain

$$\hat{\boldsymbol{x}}_{d,t} = \underset{|x_{d,m}| \leq \max(\mathcal{X})\, \forall m}{\arg\min} \; L_{\mathrm{CE}}\left(\boldsymbol{x}_{d,t}\right) \quad (38)$$

where we define $\breve{\boldsymbol{\theta}} = \frac{\breve{\boldsymbol{h}}_n}{\sigma}$ and let

$$L_{\mathrm{CE}}\left(\boldsymbol{x}_{d,t}\right) = \frac{-1}{2N} \sum_{n=1}^{2N} \left(\tfrac{y_{d,n}+1}{2}\right) \ln\left[\Phi\left(\breve{\boldsymbol{\theta}}^{\mathsf{T}} \boldsymbol{x}_d\right)\right] + \left(\tfrac{1-y_{d,n}}{2}\right) \ln\left[1 - \Phi\left(\breve{\boldsymbol{\theta}}^{\mathsf{T}} \boldsymbol{x}_d\right)\right]. \quad (39)$$

Update the gradient

$$\hat{\boldsymbol{x}}_{d,k+1} = \hat{\boldsymbol{x}}_{d,k} - \zeta_d \nabla L_{\mathrm{CE}}(\hat{\boldsymbol{x}}_{d,k}). \quad (40)$$

Finally we project on the discrete constellation.

Data detection metrics:

1. Matched maximum likelihood with perfect CSI:

$$\begin{aligned} \boldsymbol{x}_{\mathrm{ML}} &= \underset{\boldsymbol{x}\in\mathcal{X}^{2M}}{\arg\min} \quad \boldsymbol{W}(\boldsymbol{y}|\boldsymbol{x},\boldsymbol{H}) \\ &= \underset{\boldsymbol{x}\in\mathcal{X}^{2M}}{\arg\min} \quad -\sum_{n=1}^{2N} \ln\left[\Phi\left(\frac{\boldsymbol{h}_n^{\mathsf{T}}\boldsymbol{x}}{\sigma}\right)^{\frac{y_n+1}{2}} \cdot \left(1-\Phi\left(\frac{\boldsymbol{h}_n^{\mathsf{T}}\boldsymbol{x}}{\sigma}\right)\right)^{\frac{1-y_n}{2}}\right]. \end{aligned} \tag{41}$$

Channel Estimation and Data Detection with Probit Regression (4)

Data detection metrics:

1. Matched maximum likelihood with perfect CSI:

$$\begin{aligned} \boldsymbol{x}_{\mathrm{ML}} &= \underset{\boldsymbol{x} \in \mathcal{X}^{2M}}{\arg\min} \quad \boldsymbol{W}(\boldsymbol{y}|\boldsymbol{x}, \boldsymbol{H}) \\ &= \underset{\boldsymbol{x} \in \mathcal{X}^{2M}}{\arg\min} \quad -\sum_{n=1}^{2N} \ln \left[\Phi\left(\frac{\boldsymbol{h}_n^{\mathrm{T}} \boldsymbol{x}}{\sigma}\right)^{\frac{y_n+1}{2}} \cdot \left(1 - \Phi\left(\frac{\boldsymbol{h}_n^{\mathrm{T}} \boldsymbol{x}}{\sigma}\right)\right)^{\frac{1-y_n}{2}} \right]. \end{aligned} \tag{41}$$

2. Mismatched maximum likelihood (mML) using:

- Estimated parameters from the probit model

$$\hat{\boldsymbol{x}}_{\mathrm{mML}} = \underset{\boldsymbol{x} \in \mathcal{X}^{2M}}{\arg\min} \; Q(\boldsymbol{y}|\boldsymbol{x}, \hat{\boldsymbol{\Theta}}). \tag{42}$$

Data detection metrics:

1. Matched maximum likelihood with perfect CSI:

$$\begin{aligned}\boldsymbol{x}_{\mathrm{ML}} &= \underset{\boldsymbol{x}\in\mathcal{X}^{2M}}{\arg\min}\ \ \boldsymbol{W}(\boldsymbol{y}|\boldsymbol{x},\boldsymbol{H}) \\ &= \underset{\boldsymbol{x}\in\mathcal{X}^{2M}}{\arg\min}\ -\sum_{n=1}^{2N}\ln\left[\Phi\left(\frac{\boldsymbol{h}_n^{\mathrm{T}}\boldsymbol{x}}{\sigma}\right)^{\frac{y_n+1}{2}}\cdot\left(1-\Phi\left(\frac{\boldsymbol{h}_n^{\mathrm{T}}\boldsymbol{x}}{\sigma}\right)\right)^{\frac{1-y_n}{2}}\right].\end{aligned} \tag{41}$$

2. Mismatched maximum likelihood (mML) using:

- Estimated parameters from the probit model

$$\hat{\boldsymbol{x}}_{\mathrm{mML}} = \underset{\boldsymbol{x}\in\mathcal{X}^{2M}}{\arg\min}\ Q(\boldsymbol{y}|\boldsymbol{x},\hat{\boldsymbol{\Theta}}). \tag{42}$$

- Estimated parameters using the Bussgang decomposition and BLMMSE:

$$\hat{\boldsymbol{x}}_{\mathrm{BLMMSE}} = \underset{\boldsymbol{x}\in\mathcal{X}^{2M}}{\arg\min}\ Q(\boldsymbol{y}|\boldsymbol{x},\hat{\boldsymbol{H}}_{\mathrm{BLMMSE}}). \tag{43}$$

$$\hat{\boldsymbol{H}}_{\mathrm{BLMMSE}} = \frac{\alpha}{2-\frac{4}{\pi}+\tilde{\sigma}^2\alpha^2+T_p\alpha^2}\tilde{\boldsymbol{Y}}_p\tilde{\boldsymbol{X}}_p^{\mathrm{H}}, \tag{44}$$

where $\alpha = \sqrt{\frac{4}{\pi(M+\tilde{\sigma}^2)}}$.

Simulation Results: Channel Estimation and Data Detection Probit Regression (1)

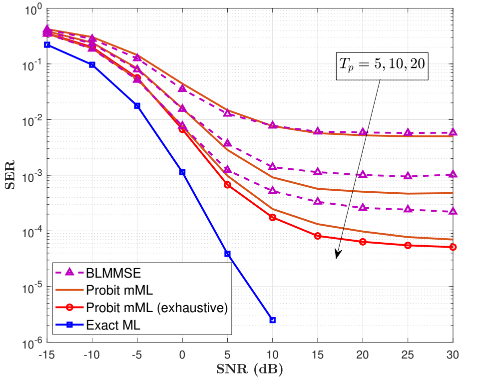

Figure: SER for exact ML, mismatched probit and BLMMSE with QPSK 4×32-MIMO and increasing training lengths $T_p = \{5, 10, 20\}$.

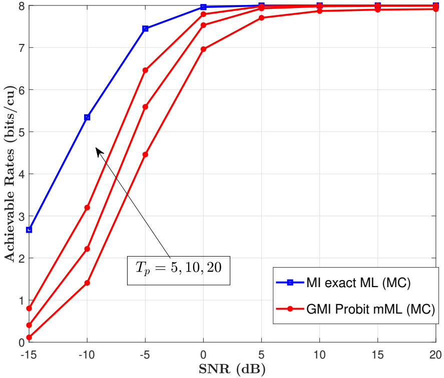

Figure: GMI for exact ML and mismatched probit model for a 4×32-MIMO with QPSK and increasing training lengths (MC simulations).

Simulation Results: Channel Estimation and Data Detection Probit Regression (2)

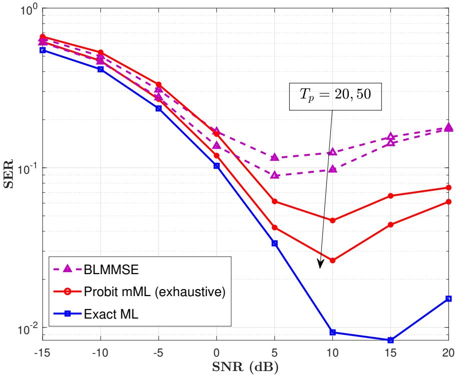

Figure: SER for exact ML, mismatched probit and BLMMSE with 16-QAM 2×32-MIMO and $T_p = \{20, 50\}$.

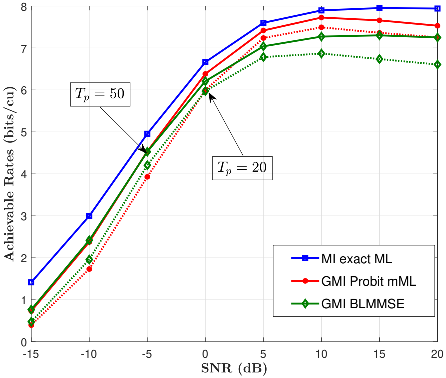

Figure: Achievable rates under the mismatched Probit and BLMMSE metrics for a 2×32-MIMO with 16-QAM and $T_p = \{20, 50\}$.

Data Detection with Statistical CSI (1)

We consider now only a real channel model: The ML data detector with statistical CSI can be written as

$$\begin{aligned} \boldsymbol{X}_d^* &= \arg\max_{\boldsymbol{X}_d} \; \boldsymbol{P}(\boldsymbol{Y}_d, \boldsymbol{Y}_p | \boldsymbol{X}_d, \boldsymbol{X}_p) \\ &= \arg\max_{\boldsymbol{X}_d} \; \mathbb{E}_{\bar{\boldsymbol{H}}} \left[\boldsymbol{P}\left(\boldsymbol{Y}_d, \boldsymbol{Y}_p | \boldsymbol{X}_d, \boldsymbol{X}_p, \bar{\boldsymbol{H}} \right) \right], \end{aligned} \tag{45}$$

Main observations

- Does not have a closed and tractable form due to the multivariate Gaussian orthant probabilities
- Optimizing over the input constellation can become prohibitive
- We can try and approximate the integration procedure
- Extend the SD approach to this metric

Data Detection with Statistical CSI (2)

Laplace approximation

$$P(\bar{H}|Y_p, X_p) \approx Q(\bar{H}|Y_p, X_p) \approx \prod_{n=1}^{N} \phi_M(\bar{h}_n; \mu_n, \Sigma_n) \approx \prod_{n=1}^{N} \frac{1}{\hat{\omega}_n} e^{-\frac{1}{2}(\bar{h}_n-\mu_n)^{\mathsf{T}}\Sigma_n^{-1}(\bar{h}_n-\mu_n)}. \quad (46)$$

The Gaussian parameters in (46) are given by

$$\begin{cases} \hat{\omega}_n = \sqrt{(2\pi)^M |\Sigma_n|} \\ \mu_n = \hat{h}_n - (\nabla^2_{\mathcal{L}(\hat{h}_n)})^{-1} \nabla_{\mathcal{L}(\hat{h}_n)} \\ \Sigma_n = -(\nabla^2_{\mathcal{L}(\hat{h}_n)})^{-1}. \end{cases} \quad (47)$$

Approximate ML metric

After averaging over the Gaussian distribution:

$$x_{\mathrm{LA}} = \arg\max_{x_d \in \mathcal{X}^M} \mathbb{E}_Q\left[P\left(y_d | x_d, \bar{H}\right)\right] = \arg\min_{x_d \in \mathcal{X}^M} -\sum_{n=1}^{N} \ln\left[\Phi\left(\frac{y_{d,n} x_d^{\mathsf{T}} \mu_n}{\sqrt{\sigma_d^2 + x_d^{\mathsf{T}} \Sigma_n x_d}}\right)\right]. \quad (48)$$

Sphere-decoding with the LA method

To alleviate the complexity of searching over the input space:

1. form the mismatched ML metric:

$$\boldsymbol{x}_{\mathrm{MM}} = \arg\min_{\boldsymbol{x}_d \in \mathcal{X}^M} -\sum_{n=1}^{N} \ln\left[\Phi\left(\frac{y_{d,n}\boldsymbol{x}_d^{\mathsf{T}}\boldsymbol{\mu}_{\boldsymbol{n}}}{\sigma_d}\right)\right]. \tag{49}$$

Sphere-decoding with the LA method

To alleviate the complexity of searching over the input space:

1. form the mismatched ML metric:

$$\boldsymbol{x}_{\mathrm{MM}} = \underset{\boldsymbol{x}_d \in \mathcal{X}^M}{\arg\min} \; -\sum_{n=1}^{N} \ln\left[\Phi\left(\frac{y_{d,n}\boldsymbol{x}_d^{\mathsf{T}}\boldsymbol{\mu}_n}{\sigma_d}\right)\right]. \tag{49}$$

2. Construct based on this metric the set

$$\mathcal{M} = \left\{[\boldsymbol{x}_1, \ldots, \boldsymbol{x}_{|\mathcal{M}|}] \in \mathcal{X}^M \mid ||\boldsymbol{t} - \boldsymbol{U}\boldsymbol{x}_k||^2 \leq d\right\}. \tag{50}$$

Sphere-decoding with the LA method

To alleviate the complexity of searching over the input space:

1. form the mismatched ML metric:

$$\boldsymbol{x}_{\text{MM}} = \underset{\boldsymbol{x}_d \in \mathcal{X}^M}{\arg\min} \; -\sum_{n=1}^{N} \ln \left[\Phi \left(\frac{y_{d,n} \boldsymbol{x}_d^{\text{T}} \boldsymbol{\mu}_{\boldsymbol{n}}}{\sigma_d} \right) \right]. \tag{49}$$

2. Construct based on this metric the set

$$\mathcal{M} = \left\{ [\boldsymbol{x}_1, \ldots, \boldsymbol{x}_{|\mathcal{M}|}] \in \mathcal{X}^M \mid ||\boldsymbol{t} - \boldsymbol{U}\boldsymbol{x}_k||^2 \leq d \right\}. \tag{50}$$

3. Finally, we perform the optimization

$$\boldsymbol{x}_{\text{LA-SD}} = \underset{\boldsymbol{x}_d \in \mathcal{M}}{\arg\min} \; -\sum_{n=1}^{N} \ln \left[\Phi \left(\frac{y_{d,n} \boldsymbol{x}_d^{\text{T}} \boldsymbol{\mu}_{\boldsymbol{n}}}{\sqrt{\sigma_d + \boldsymbol{x}_d^{\text{T}} \boldsymbol{\Sigma}_n \boldsymbol{x}_d}} \right) \right]. \tag{51}$$

Simulation Results:Data Detection with Statistical CSI

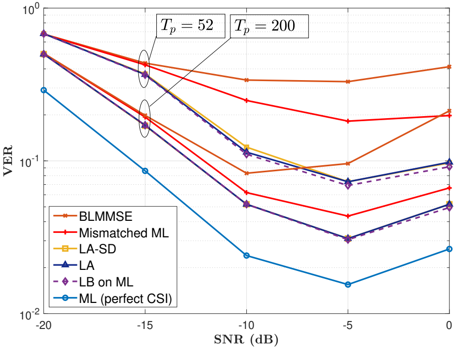

Figure: VER for a 2×64 real MIMO system with varying SNR and increasing T_p.

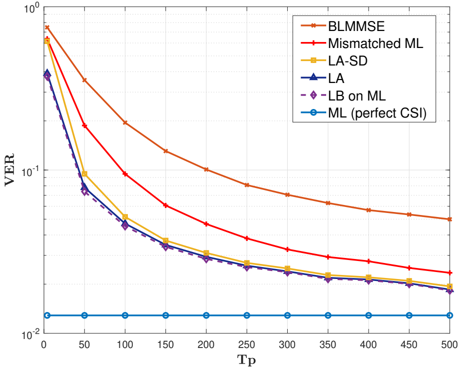

Figure: VER performance with respect to increasing training lengths for a 2×64 real MIMO channel, 4-PAM signaling, SNR is fixed to -5dB, and $|\mathcal{M}| = 2$ points.

Current Section

Work in progress

- Investigating the energy efficiency-rate tradeoff
- Obtaining a characterization of the capacity
- Applying results by Clarke and Barron [CB94]
- Unquantized non-coherent channel for special cases $T = 1, 2$ and 3.
- Coherent multi-bit quantized channel

Improvements and extensions

Future work considers

- Oversampling in the extreme case of one-bit ADCs
- Constraint on the transmission with low-resolution digital-to-analog converters: precoding strategies
- More general frequency-selective channels and OFDM transmission
- Analyzing analytically the SD complexity
- Extending LA method to the complex channel model

Exploring other sources of nonlinearities

- Exploring effects of aperture uncertainty when sampling
- PA distortion
- Phase noise effects and I/Q imbalancing

Thank you

References

[Agr+02] E. Agrell et al. "Closest point search in lattices". en. In: *IEEE Transactions on Information Theory* 48.8 (Aug. 2002), pp. 2201–2214.

[AT22] Italo Atzeni and Antti Tolli. "Channel Estimation and Data Detection Analysis of Massive MIMO With 1-Bit ADCs". en. In: *IEEE Transactions on Wireless Communications* 21.6 (June 2022), pp. 3850–3867.

[Bin+05] Bin Le et al. "Analog-to-digital converters". en. In: *IEEE Signal Processing Magazine* 22.6 (Nov. 2005), pp. 69–77.

[CB94] Bertrand S. Clarke and Andrew R. Barron. "Jeffreys' prior is asymptotically least favorable under entropy risk". en. In: *Journal of Statistical Planning and Inference* 41.1 (Aug. 1994), pp. 37–60.

[CMH16] Junil Choi, Jianhua Mo, and Robert W. Heath. "Near Maximum-Likelihood Detector and Channel Estimator for Uplink Multiuser Massive MIMO Systems With One-Bit ADCs". en. In: *IEEE Transactions on Communications* 64.5 (May 2016), pp. 2005–2018.

[CY18] Richard Combes and Sheng Yang. "An Approximate ML Detector for MIMO Channels Corrupted by Phase Noise". en. In: *IEEE Transactions on Communications* 66.3 (Mar. 2018), pp. 1176–1189.

[Jac+17] Sven Jacobsson et al. "Throughput Analysis of Massive MIMO Uplink With Low-Resolution ADCs". en. In: *IEEE Transactions on Wireless Communications* 16.6 (June 2017), pp. 4038–4051.

[Jeo+18] Yo-Seb Jeon et al. "One-Bit Sphere Decoding for Uplink Massive MIMO Systems With One-Bit ADCs". en. In: *IEEE Transactions on Wireless Communications* 17.7 (July 2018), pp. 4509–4521.

References

[Jeo+22] Yo-Seb Jeon et al. "Artificial Intelligence for Physical-Layer Design of MIMO Communications with One-Bit ADCs". en. In: *IEEE Communications Magazine* 60.7 (July 2022), pp. 76–81.

[Kho+21] Shahin Khobahi et al. "Model-Inspired Deep Detection with Low-Resolution Receivers". en. In: *2021 IEEE International Symposium on Information Theory (ISIT)*. Melbourne, Australia: IEEE, July 2021, pp. 3349–3354.

[LR23] Angel Lozano and Sundeep Rangan. *Spectral vs Energy Efficiency in 6G: Impact of the Receiver Front-End*. en. arXiv:2310.02622 [cs, eess, math]. Oct. 2023.

[MNS20] Amine Mezghani, Josef A. Nossek, and A. Lee Swindlehurst. "Low SNR Asymptotic Rates of Vector Channels With One-Bit Outputs". en. In: *IEEE Transactions on Information Theory* 66.12 (Dec. 2020), pp. 7615–7634.

[Mur15] Boris Murmann. "The Race for the Extra Decibel: A Brief Review of Current ADC Performance Trajectories". en. In: *IEEE Solid-State Circuits Magazine* 7.3 (2015), pp. 58–66.

[NSN21a] Ly V. Nguyen, A. Lee Swindlehurst, and Duy H. N. Nguyen. "Linear and Deep Neural Network-Based Receivers for Massive MIMO Systems With One-Bit ADCs". en. In: *IEEE Transactions on Wireless Communications* 20.11 (Nov. 2021), pp. 7333–7345.

[NSN21b] Ly V. Nguyen, A. Lee Swindlehurst, and Duy H. N. Nguyen. "SVM-Based Channel Estimation and Data Detection for One-Bit Massive MIMO Systems". en. In: *IEEE Transactions on Signal Processing* 69 (2021), pp. 2086–2099.

[OER15] Oner Orhan, Elza Erkip, and Sundeep Rangan. "Low power analog-to-digital conversion in millimeter wave systems: Impact of resolution and bandwidth on performance". en. In: *2015 Information Theory and Applications Workshop (ITA)*. San Diego, CA, USA: IEEE, Feb. 2015, pp. 191–198.

References

[QAN13] Bai Qing, Mezghani Amine, and Josef A. Nossek. "On the Optimization of ADC Resolution in Multi-antenna Systems". In: *2013 The Tenth International Symposium on Wireless Communication Systems*. VDE, 2013, pp. 1–5.

[SD16] Christoph Studer and Giuseppe Durisi. "Quantized Massive MU-MIMO-OFDM Uplink". en. In: *IEEE Transactions on Communications* 64.6 (June 2016), pp. 2387–2399.

[SDM09] Jaspreet Singh, Onkar Dabeer, and Upamanyu Madhow. "On the limits of communication with low-precision analog-to-digital conversion at the receiver". en. In: *IEEE Transactions on Communications* 57.12 (Dec. 2009), pp. 3629–3639.

[Wal99] R.H. Walden. "Analog-to-digital converter survey and analysis". en. In: *IEEE Journal on Selected Areas in Communications* 17.4 (Apr. 1999), pp. 539–550.

[Wen+16] Chao-Kai Wen et al. "Bayes-Optimal Joint Channel-and-Data Estimation for Massive MIMO With Low-Precision ADCs". en. In: *IEEE Transactions on Signal Processing* 64.10 (May 2016), pp. 2541–2556.

[YC24a] Sheng Yang and Richard Combes. *Asymptotic Capacity of 1-Bit MIMO Fading Channels*. en. arXiv:2407.16242 [cs, math]. July 2024.

[YC24b] Sheng Yang and Richard Combes. "Asymptotic Capacity of Non-Coherent One-Bit MIMO Channels with Block Fading". en. In: *2024 IEEE International Symposium on Information Theory (ISIT)*. Athens, Greece: IEEE, July 2024, pp. 2359–2364.

RF Impairments: PA Distortion

PA distortion:

- Generally characterized by the Volterra series operator $V[\cdot]$ with set of causal kernels h_n, given a real-time domain signal $x(t)$:

$$y(t) = \mathrm{V}\left[x(t)\right] = \sum_{n=0}^{\infty} \int_{0}^{\infty} \dots \int_{0}^{\infty} h_n(\tau_1, \dots, \tau_n) \prod_{i=1}^{n} x(t - \tau_i)\, \mathrm{d}\tau_i$$

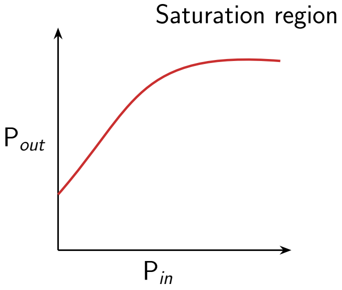

Figure: PA nonlinear power characteristic

PA distortion:

- Generally characterized by the Volterra series operator $V[\cdot]$ with set of causal kernels h_n, given a real-time domain signal $x(t)$:

$$\begin{aligned} y(t) &= \mathrm{V}\left[x(t)\right] \\ &= \sum_{n=0}^{\infty} \int_{0}^{\infty} \dots \int_{0}^{\infty} h_n(\tau_1, \dots, \tau_n) \prod_{i=1}^{n} x(t - \tau_i)\,\mathrm{d}\tau_i \end{aligned}$$

- Amplitude-to-amplitude (AM-AM) and amplitude-to-phase modulation (AM-PM)

$$y(t) = \underbrace{G(|\tilde{x}(t)|)}_{\text{AM-AM}} \cos\left(2\pi f_c t + \phi(t) + \underbrace{\Psi(|\tilde{x}(t)|)}_{\text{AM-PM}}\right)$$

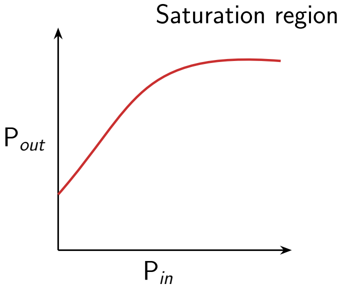

Figure: PA nonlinear power characteristic

Bussgang Decomposition (1)

There are several approaches that handle the nonlinearity

Channel Linearization

The Bussgang decomposition, given the input-output relationship

$$\boldsymbol{v} = f(\boldsymbol{u}). \tag{52}$$

By restricting to the class of linear estimators, the output can be written

$$\begin{aligned} \boldsymbol{v} &= \boldsymbol{W}\boldsymbol{u} + \boldsymbol{e} \\ &= \mathbb{E}\left[\boldsymbol{v}\boldsymbol{u}^{\mathrm{H}}\right] \mathbb{E}\left[\boldsymbol{u}\boldsymbol{u}^{\mathrm{H}}\right]^{-1} \boldsymbol{u} + \boldsymbol{e}. \end{aligned} \tag{53}$$

By the orthogonality principle, the noise term $\boldsymbol{e}$ is uncorrelated with the input but not independent.

Bussgang Decomposition (2)

Letting $\tilde{\boldsymbol{r}} = \tilde{\boldsymbol{H}}\tilde{\boldsymbol{x}} + \tilde{\boldsymbol{z}}$ applying this result to our channel model we obtain

Bussgang decomposition for quantized channel

$$\begin{aligned}\tilde{\boldsymbol{y}} &= \boldsymbol{W}_b\tilde{\boldsymbol{r}} + \boldsymbol{e} \\ &= \boldsymbol{W}_b\tilde{\boldsymbol{H}}\tilde{\boldsymbol{x}} + \boldsymbol{W}_b\tilde{\boldsymbol{z}} + \boldsymbol{e} \\ &= \tilde{\boldsymbol{G}}_b\tilde{\boldsymbol{x}} + \tilde{\boldsymbol{n}} \end{aligned} \tag{54}$$

where $\boldsymbol{W}_b$ is equal to

$$\mathrm{diag}(\boldsymbol{C}_{\tilde{\boldsymbol{r}}})^{-\frac{1}{2}} \sum_{i=1}^{2^b} \frac{\nu_i}{\sqrt{\pi}} \left(e^{-l_{i-1}^2 \mathrm{diag}(\boldsymbol{C}_{\tilde{\boldsymbol{r}}})^{-1}} - e^{-l_i^2 \mathrm{diag}(\boldsymbol{C}_{\tilde{\boldsymbol{r}}})^{-1}} \right). \tag{55}$$

The input is assumed Gaussian with covariance $\boldsymbol{C}_{\tilde{\boldsymbol{r}}}$.

Using this decomposition, we obtain linear receivers and estimators in the following form

Linear receivers

$$\hat{\boldsymbol{x}} = \boldsymbol{F}\tilde{\boldsymbol{y}}. \tag{56}$$

- Bussgang Maximum Ratio Combining:

$$\boldsymbol{F}_{\mathrm{BMRC}} = \mathrm{diag}\left(\tilde{\boldsymbol{G}}_b^{\mathrm{H}}\tilde{\boldsymbol{G}}_b\right)^{-1}\tilde{\boldsymbol{G}}_b^{\mathrm{H}}. \tag{57}$$

- Bussgang ZF receiver

$$\boldsymbol{F}_{\mathrm{BZF}} = \left(\tilde{\boldsymbol{G}}_b^{\mathrm{H}}\tilde{\boldsymbol{G}}_b\right)^{-1}\tilde{\boldsymbol{G}}_b^{\mathrm{H}}. \tag{58}$$

- Bussgang MMSE (BMMSE)

$$\boldsymbol{F}_{\mathrm{BMMSE}} = \tilde{\boldsymbol{G}}_b^{\mathrm{H}}\boldsymbol{C}_{\tilde{\boldsymbol{y}}}^{-1}. \tag{59}$$

ML detection in unquantized channel

Assume we have infinite precision

$$\boldsymbol{r} = \boldsymbol{H}\boldsymbol{x} + \boldsymbol{z}. \tag{60}$$

Translate the constellation to a subset $\mathcal{D} \subset \mathbb{Z}^{2M}$ where

$$\mathcal{D} = \left\{ \boldsymbol{s} = \frac{1}{2}(\boldsymbol{x} + \mathbf{1}_{2M}) : \boldsymbol{x} \in \mathcal{X}^{2M} \right\}. \tag{61}$$

$$\boldsymbol{s}_{\text{ML}} = \arg\min_{\boldsymbol{s}\in\mathcal{D}} \quad ||\boldsymbol{t} - \boldsymbol{B}\boldsymbol{s}||^2, \tag{62}$$

where $\boldsymbol{B} = 2\boldsymbol{H}$ and $\boldsymbol{t} = \boldsymbol{y} + \boldsymbol{H}\mathbf{1}_{2M} \in \mathbb{R}^{2N}$. $\boldsymbol{B}$ is usually referred to as the *lattice-generating matrix* [Agr+02], i.e., we have the truncated lattice $\Gamma = \{\boldsymbol{B}\boldsymbol{s} : \boldsymbol{s} \in \mathcal{D}\}$

Integer least-squares problem

Constrain the search over a sphere of radius d

$$\left\{ \boldsymbol{s} \in \mathcal{D} : ||\boldsymbol{t} - \boldsymbol{B}\boldsymbol{s}||^2 \leq d \right\}. \tag{63}$$

$$\boldsymbol{B} = \boldsymbol{Q}\boldsymbol{R} = \begin{bmatrix} \boldsymbol{Q}_1 & \boldsymbol{Q}_2 \end{bmatrix} \begin{bmatrix} \boldsymbol{R}_1 \\ \mathbf{0} \end{bmatrix} \tag{64}$$

$$\begin{aligned} \boldsymbol{s}_{\text{ML}} &= \arg\min_{\boldsymbol{s}\in\mathcal{D}} \quad ||\boldsymbol{t} - \boldsymbol{B}\boldsymbol{s}||^2 \\ &= \arg\min_{\boldsymbol{s}\in\mathcal{D}} \quad ||\boldsymbol{R}_1\boldsymbol{s}_{\text{ZF}} - \boldsymbol{R}_1\boldsymbol{s}||^2 + c \\ &= \arg\min_{\boldsymbol{s}\in\mathcal{D}} \quad ||\hat{\boldsymbol{t}} - \boldsymbol{R}_1\boldsymbol{s}||^2 \end{aligned} \tag{65}$$

where $\boldsymbol{s}_{\text{ZF}} = (\boldsymbol{B}^{\mathsf{T}}\boldsymbol{B})^{-1}\boldsymbol{B}^{\mathsf{T}}\boldsymbol{t}$ is the ZF estimate.

ML Lowerbound and nML approach

Lowerbound on ML

Given a sub-optimal solution $\boldsymbol{x}^{\dagger}$ and an oracle that can provide us with the transmitted vector $\boldsymbol{x}$ and an optimal metric $\boldsymbol{q}(\boldsymbol{x})$, the ML error probability can be lower bounded as [CY18]:

$$\boldsymbol{P}_{\mathrm{ML}}(\text{error}) \geq \boldsymbol{P}\left\{\boldsymbol{x} \neq \boldsymbol{x}^{\dagger},\, \boldsymbol{q}(\boldsymbol{x}) < \boldsymbol{q}(\boldsymbol{x}^{\dagger})\right\}, \tag{66}$$

Near-ML approach [CMH16]

1. In the first stage, the metric

$$\underset{\substack{\boldsymbol{x}\in\mathbb{R}^{2M} \\ ||\boldsymbol{x}||^2 \leq M}}{\arg\min} \; -\sum_{n=1}^{2N} \ln\left[\Phi\left(\frac{y_n \boldsymbol{h}_n^{\mathrm{T}} \boldsymbol{x}}{\sigma}\right)\right] \tag{67}$$

ML Lowerbound and nML approach

Lowerbound on ML

Given a sub-optimal solution $\boldsymbol{x}^\dagger$ and an oracle that can provide us with the transmitted vector $\boldsymbol{x}$ and an optimal metric $\boldsymbol{q}(\boldsymbol{x})$, the ML error probability can be lower bounded as [CY18]:

$$\boldsymbol{P}_{\mathrm{ML}}(\mathrm{error}) \geq \boldsymbol{P}\left\{\boldsymbol{x} \neq \boldsymbol{x}^\dagger,\, \boldsymbol{q}(\boldsymbol{x}) < \boldsymbol{q}(\boldsymbol{x}^\dagger)\right\}, \tag{66}$$

Near-ML approach [CMH16]

1. In the first stage, the metric

$$\underset{\substack{\boldsymbol{x}\in\mathbb{R}^{2M} \\ ||\boldsymbol{x}||^2 \leq M}}{\arg\min} \; -\sum_{n=1}^{2N} \ln\left[\Phi\left(\frac{y_n \boldsymbol{h}_n^{\mathrm{T}} \boldsymbol{x}}{\sigma}\right)\right] \tag{67}$$

2. Normalize to obtain $\dot{\boldsymbol{x}}_{\mathrm{nML}}$

ML Lowerbound and nML approach

Lowerbound on ML

Given a sub-optimal solution $\boldsymbol{x}^\dagger$ and an oracle that can provide us with the transmitted vector $\boldsymbol{x}$ and an optimal metric $\boldsymbol{q}(\boldsymbol{x})$, the ML error probability can be lower bounded as [CY18]:

$$\boldsymbol{P}_{\mathrm{ML}}(\text{error}) \geq \boldsymbol{P}\left\{\boldsymbol{x} \neq \boldsymbol{x}^\dagger,\ \boldsymbol{q}(\boldsymbol{x}) < \boldsymbol{q}(\boldsymbol{x}^\dagger)\right\}, \tag{66}$$

Near-ML approach [CMH16]

1. In the first stage, the metric

$$\underset{\substack{\boldsymbol{x}\in\mathbb{R}^{2M} \\ ||\boldsymbol{x}||^2 \leq M}}{\arg\min} \; -\sum_{n=1}^{2N} \ln\left[\Phi\left(\frac{y_n \boldsymbol{h}_n^{\mathrm{T}} \boldsymbol{x}}{\sigma}\right)\right] \tag{67}$$

2. Normalize to obtain $\dot{\boldsymbol{x}}_{\mathrm{nML}}$
3. Map back to $\mathcal{X}^{2M}$ symbol-by-symbol and obtain $\ddot{\boldsymbol{x}}_{\mathrm{nML}}$

ML Lowerbound and nML approach

Lowerbound on ML

Given a sub-optimal solution $\boldsymbol{x}^\dagger$ and an oracle that can provide us with the transmitted vector $\boldsymbol{x}$ and an optimal metric $\boldsymbol{q}(\boldsymbol{x})$, the ML error probability can be lower bounded as [CY18]:

$$\boldsymbol{P}_{\mathrm{ML}}(\text{error}) \geq \boldsymbol{P}\left\{\boldsymbol{x} \neq \boldsymbol{x}^\dagger,\ \boldsymbol{q}(\boldsymbol{x}) < \boldsymbol{q}(\boldsymbol{x}^\dagger)\right\}, \tag{66}$$

Near-ML approach [CMH16]

1. In the first stage, the metric

$$\underset{\substack{\boldsymbol{x}\in\mathbb{R}^{2M} \\ ||\boldsymbol{x}||^2 \leq M}}{\arg\min} \; -\sum_{n=1}^{2N} \ln\left[\Phi\left(\frac{y_n \boldsymbol{h}_n^{\mathrm{T}} \boldsymbol{x}}{\sigma}\right)\right] \tag{67}$$

2. Normalize to obtain $\dot{\boldsymbol{x}}_{\mathrm{nML}}$
3. Map back to $\mathcal{X}^{2M}$ symbol-by-symbol and obtain $\ddot{\boldsymbol{x}}_{\mathrm{nML}}$
4. Fix $\chi > 1$ is fixed, then construct $\forall m$

$$\mathcal{C}_m = \left\{x \in \tilde{\mathcal{X}} \,\middle|\, \frac{|\dot{x}_m - x|}{|\dot{x}_m - \ddot{x}_m|} < \chi\right\}, \tag{68}$$

ML Lowerbound and nML approach

Lowerbound on ML

Given a sub-optimal solution $\boldsymbol{x}^{\dagger}$ and an oracle that can provide us with the transmitted vector $\boldsymbol{x}$ and an optimal metric $\boldsymbol{q}(\boldsymbol{x})$, the ML error probability can be lower bounded as [CY18]:

$$\boldsymbol{P}_{\mathrm{ML}}(\text{error}) \geq \boldsymbol{P}\left\{\boldsymbol{x} \neq \boldsymbol{x}^{\dagger},\ \boldsymbol{q}(\boldsymbol{x}) < \boldsymbol{q}(\boldsymbol{x}^{\dagger})\right\}, \tag{66}$$

Near-ML approach [CMH16]

1. In the first stage, the metric

$$\underset{\substack{\boldsymbol{x}\in\mathbb{R}^{2M} \\ ||\boldsymbol{x}||^2\leq M}}{\arg\min} -\sum_{n=1}^{2N} \ln\left[\Phi\left(\frac{y_n \boldsymbol{h}_n^{\mathrm{T}}\boldsymbol{x}}{\sigma}\right)\right] \tag{67}$$

2. Normalize to obtain $\dot{\boldsymbol{x}}_{\mathrm{nML}}$
3. Map back to $\mathcal{X}^{2M}$ symbol-by-symbol and obtain $\ddot{\boldsymbol{x}}_{\mathrm{nML}}$
4. Fix $\chi > 1$ is fixed, then construct $\forall m$

$$\mathcal{C}_m = \left\{x \in \tilde{\mathcal{X}} \,\middle|\, \frac{|\dot{x}_m - x|}{|\dot{x}_m - \ddot{x}_m|} < \chi\right\}, \tag{68}$$

5. Then form $\mathcal{C} = \mathcal{C}_1 \times \mathcal{C}_2 \times \cdots \times \mathcal{C}_M$, such that

$$\mathcal{C} = \left\{\check{\boldsymbol{x}} = [\check{x}_1, \ldots, \check{x}_m, \ldots, \check{x}_M]^{\mathrm{T}} \,\middle|\, \check{x}_m \in \mathcal{C}_m, \forall m\right\}. \tag{69}$$

ML Lowerbound and nML approach

Lowerbound on ML

Given a sub-optimal solution $\boldsymbol{x}^\dagger$ and an oracle that can provide us with the transmitted vector $\boldsymbol{x}$ and an optimal metric $\boldsymbol{q}(\boldsymbol{x})$, the ML error probability can be lower bounded as [CY18]:

$$\boldsymbol{P}_{\text{ML}}(\text{error}) \geq \boldsymbol{P}\left\{\boldsymbol{x} \neq \boldsymbol{x}^\dagger,\, \boldsymbol{q}(\boldsymbol{x}) < \boldsymbol{q}(\boldsymbol{x}^\dagger)\right\}, \tag{66}$$

Near-ML approach [CMH16]

1. In the first stage, the metric

$$\underset{\substack{\boldsymbol{x}\in\mathbb{R}^{2M} \\ ||\boldsymbol{x}||^2 \leq M}}{\arg\min} \; -\sum_{n=1}^{2N} \ln\left[\Phi\left(\frac{y_n \boldsymbol{h}_n^{\mathsf{T}} \boldsymbol{x}}{\sigma}\right)\right] \tag{67}$$

2. Normalize to obtain $\dot{\boldsymbol{x}}_{\text{nML}}$
3. Map back to $\mathcal{X}^{2M}$ symbol-by-symbol and obtain $\ddot{\boldsymbol{x}}_{\text{nML}}$
4. Fix $\chi > 1$ is fixed, then construct $\forall m$

$$\mathcal{C}_m = \left\{x \in \tilde{\mathcal{X}} \,\middle|\, \frac{|\dot{x}_m - x|}{|\dot{x}_m - \ddot{x}_m|} < \chi\right\}, \tag{68}$$

5. Then form $\mathcal{C} = \mathcal{C}_1 \times \mathcal{C}_2 \times \cdots \times \mathcal{C}_M$, such that

$$\mathcal{C} = \left\{\check{\boldsymbol{x}} = [\check{x}_1, \ldots, \check{x}_m, \ldots, \check{x}_M]^{\mathsf{T}} \,\middle|\, \check{x}_m \in \mathcal{C}_m, \forall m\right\}. \tag{69}$$

6. The nML solution is finally obtained as

$$\boldsymbol{x}_{\text{nML}} = \underset{\boldsymbol{x}\in\mathcal{C}}{\arg\max}\; \ell_1(\boldsymbol{x}). \tag{70}$$

Functions Required

Given, an initial estimate $\boldsymbol{x}_0$, form the Taylor series approximation

$$\ell(\boldsymbol{x}) = \ell(\boldsymbol{x}_0) + (\boldsymbol{x} - \boldsymbol{x}_0)^{\mathsf{T}} \nabla_{\ell(\boldsymbol{x}_0)} + \frac{1}{2}(\boldsymbol{x} - \boldsymbol{x}_0)^{\mathsf{T}} \nabla^2_{\ell(\boldsymbol{x}_0)} (\boldsymbol{x} - \boldsymbol{x}_0) \tag{71}$$

$$\begin{cases} \nabla_{\ell(\boldsymbol{x})} = \dfrac{\partial \ell(\boldsymbol{x})}{\partial \boldsymbol{x}} = -\dfrac{1}{\sigma} \displaystyle\sum_{n=1}^{2N} \kappa\left(\dfrac{y_n \boldsymbol{h}_n^{\mathsf{T}} \boldsymbol{x}}{\sigma}\right) y_n \boldsymbol{h}_n, & (72) \\ \nabla^2_{\ell(\boldsymbol{x})} = \dfrac{\partial^2 \ell(\boldsymbol{x})}{\partial \boldsymbol{x}^2} = \dfrac{1}{\sigma^2} \displaystyle\sum_{n=1}^{2N} \eta\left(\dfrac{y_n \boldsymbol{h}_n^{\mathsf{T}} \boldsymbol{x}}{\sigma}\right) \boldsymbol{h}_n \boldsymbol{h}_n^{\mathsf{T}}, & (73) \end{cases}$$

where we define the following functions for convenience

$$\begin{cases} \kappa(u) = \dfrac{\phi(u)}{\Phi(u)}, & (74) \\ \eta(u) = \kappa(u)\left[u + \kappa(u)\right]. & (75) \end{cases}$$

Simulation Results (3)

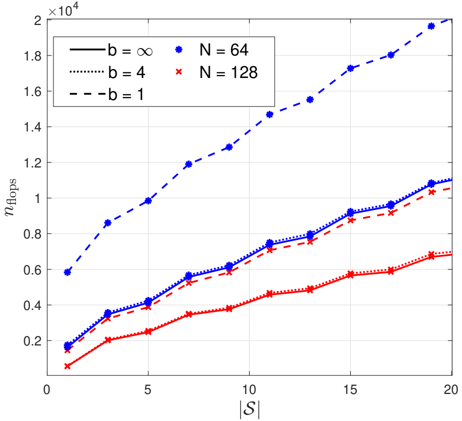

Figure: Scaling of average floating point operations with list size $|\mathcal{S}|$ in a $8 \times N$-MIMO system, 16-QAM with $M = 8$, SNR=-5 dB, and different assumptions on b and N.

Table
Average number of iterations K_{SD} and K_{nML} with $b = 1$, different assumptions on the SNR, constellation size, and antenna configurations.

	$\rho = -10$ dB		$\rho = 10$ dB	
	K_{SD}	K_{nML}	K_{SD}	K_{nML}
QPSK, $M = 8, N = 64$	35.7	44.5	198.3	313.[illegible]
16-QAM, $M = 4, N = 64$	32.9	64.1	153.9	267.[illegible]
16-QAM, $M = 8, N = 128$	44.6	49.7	193.3	307.[illegible]

Assuming we detect at each time instant t independently, re-write

$$\begin{aligned} \boldsymbol{x}_d^* &= \underset{\boldsymbol{x}_d \in \mathcal{X}^M}{\arg\max}\ \mathbb{E}\left[\boldsymbol{P}(\boldsymbol{y}_d|\boldsymbol{x}_d, \bar{\boldsymbol{H}}) \cdot \boldsymbol{P}(\boldsymbol{Y}_p|\boldsymbol{X}_p, \bar{\boldsymbol{H}})\right] \\ &= \underset{\boldsymbol{x}_d \in \mathcal{X}^M}{\arg\max} \int \boldsymbol{P}(\boldsymbol{y}_d|\boldsymbol{x}_d, \bar{\boldsymbol{H}}) \cdot \boldsymbol{P}(\boldsymbol{Y}_p|\boldsymbol{X}_p, \bar{\boldsymbol{H}}) \cdot \boldsymbol{P}(\bar{\boldsymbol{H}})\,\mathrm{d}\bar{\boldsymbol{H}} \\ &= \underset{\boldsymbol{x}_d \in \mathcal{X}^M}{\arg\max}\ \mathbb{E}_{\bar{\boldsymbol{H}}|\boldsymbol{Y}_p, \boldsymbol{X}_p}\left[\boldsymbol{P}(\boldsymbol{y}_d|\boldsymbol{x}_d, \bar{\boldsymbol{H}})\right]. \end{aligned} \tag{76}$$

From Bayes' theorem, we can write

$$\begin{aligned} \boldsymbol{P}(\bar{\boldsymbol{H}}|\boldsymbol{Y}_p \boldsymbol{X}_p) &= \prod_{n=1}^{N} \boldsymbol{P}(\bar{\boldsymbol{h}}_n|\boldsymbol{Y}_p, \boldsymbol{X}_p) \\ &= \prod_{n=1}^{N} \left[\frac{1}{\boldsymbol{\omega}_n} \boldsymbol{P}(\boldsymbol{y}_{p,n}|\boldsymbol{X}_p, \bar{\boldsymbol{h}}_n) \cdot \boldsymbol{P}(\bar{\boldsymbol{h}}_n)\right] \\ &= \prod_{n=1}^{N} \left[\frac{1}{\boldsymbol{\omega}_n} \prod_{t=1}^{T_p} \Phi\left(\frac{y_{p,n}^t \bar{\boldsymbol{h}}_n^\top \boldsymbol{x}_{p,t}}{\sigma_p}\right) \cdot \boldsymbol{P}(\bar{\boldsymbol{h}}_n)\right], \end{aligned} \tag{77}$$

where

$$\boldsymbol{\Omega} = \prod_{n=1}^{N} \boldsymbol{\omega}_n, \text{ and } \boldsymbol{\omega}_n = \int \prod_{t=1}^{T_p} \Phi\left(\frac{y_{p,n}^t \bar{\boldsymbol{h}}_n^\top \boldsymbol{x}_{p,t}}{\sigma_p}\right) \cdot \boldsymbol{P}(\bar{\boldsymbol{h}}_n)\,\mathrm{d}\boldsymbol{h}_n. \tag{78}$$

System model

The mutual information is given by

$$C = \max_{P_{\boldsymbol{X}} \in \mathcal{P}} \boldsymbol{I}(P_{\boldsymbol{X}}; P_{\boldsymbol{Y}|\boldsymbol{X}}), \tag{79}$$

Introduce the following Markov chain:

$$\boldsymbol{X} \to \boldsymbol{\theta} \to \boldsymbol{Y}, \tag{80}$$

$$\boldsymbol{\Theta} = \{\boldsymbol{\theta}(\boldsymbol{X}) : \boldsymbol{X} \in \mathcal{X}\} \subseteq \mathbb{R}^d. \tag{81}$$

Applying the data processing inequality we have

$$I(P_{\boldsymbol{X}}; P_{\boldsymbol{Y}|\boldsymbol{X}}) \leq I(P_{\boldsymbol{\theta}}, f_{\boldsymbol{\theta}}), \tag{82}$$

Asymptotic Capacity using Barron and Clarke's Results

System model

The mutual information is given by

$$C = \max_{P_{\boldsymbol{X}} \in \mathcal{P}} \boldsymbol{I}(P_{\boldsymbol{X}}; P_{\boldsymbol{Y}|\boldsymbol{X}}), \tag{79}$$

Introduce the following Markov chain:

$$\boldsymbol{X} \to \boldsymbol{\theta} \to \boldsymbol{Y}, \tag{80}$$

$$\boldsymbol{\Theta} = \{\boldsymbol{\theta}(\boldsymbol{X}) : \boldsymbol{X} \in \mathcal{X}\} \subseteq \mathbb{R}^d. \tag{81}$$

Applying the data processing inequality we have

$$I(P_{\boldsymbol{X}}; P_{\boldsymbol{Y}|\boldsymbol{X}}) \leq I(P_{\boldsymbol{\theta}}, f_{\boldsymbol{\theta}}), \tag{82}$$

Asymptotic capacity

The capacity can be upper-bounded as

$$\begin{aligned} C \leq \underbrace{\sup_{P_{\boldsymbol{\theta}}} \inf_{\boldsymbol{Q}} D(f_{\boldsymbol{\theta}}||\boldsymbol{Q}|P_{\boldsymbol{\theta}})}_{\underline{C}_N} &\overset{(a)}{\leq} \inf_{\boldsymbol{Q}} \sup_{P_{\boldsymbol{\theta}}} D(f_{\boldsymbol{\theta}}||\boldsymbol{Q}|P_{\boldsymbol{\theta}}) \\ &= \underbrace{\inf_{\boldsymbol{Q}} \sup_{\boldsymbol{\theta}} D(f_{\boldsymbol{\theta}}||\boldsymbol{Q})}_{\bar{C}_N} \end{aligned} \tag{83}$$

Clarke and Barron's theorem [CB94] shows that asymptotically

$$\lim_{N\to\infty} \left[\bar{C}_N - \frac{d}{2}\log\frac{N}{2\pi e}\right] = \log \int_{\boldsymbol{\theta}} |J(\boldsymbol{\theta})|^{\frac{1}{2}} \, \mathrm{d}\boldsymbol{\theta}, \tag{84}$$

$$\lim_{N\to\infty} \left[\underline{C}_N - \frac{d}{2}\log\frac{N}{2\pi e}\right] = \log \int_{\boldsymbol{\theta}} |J(\boldsymbol{\theta})|^{\frac{1}{2}} \, \mathrm{d}\boldsymbol{\theta}. \tag{85}$$

Coherent channel with multi-bit ADCS

The result of Clarke and Barron has been applied for this channel in [YC24a; YC24b] and can be extended in the same way to the multi-bit case to obtain the capacity scaling. The

$$C = \frac{M}{2}\log\frac{N}{2\pi e} + \log\alpha_{\rho,M}^{b,\delta} + \log V_M + o(1) \tag{86}$$

where

$$\alpha_{\rho,M}^{b,\delta} = \int_0^{\sqrt{\rho}} \zeta_0^{b,\delta}(r)^{\frac{M-1}{2}} \zeta_2^{b,\delta}(r)^{\frac{1}{2}} r^{M-1}\,\mathrm{d}r, \tag{87}$$

and

$$\xi_{b,\delta}(s) = \sum_{\mathrm{y}=1}^{2^b} \frac{(\phi(I_{\mathrm{y}}-s)-\phi(I_{\mathrm{y}-1}-s))^2}{\Phi(I_{\mathrm{y}}-s)-\Phi(I_{\mathrm{y}-1}-s)}, \tag{88}$$

, and V_M is the volume of a unit ball with dimension M.

Application of Clarke and Barron's Results: Unquantized Non-Coherent Channel (1)

Unquantized non-coherent channel

Assuming infinite precision, the channel likelihood is given by

$$p(\boldsymbol{Y}|\boldsymbol{X}) = \prod_{n=1}^{N} p(\boldsymbol{y}_n|\boldsymbol{X}), \tag{89}$$

where we have N i.i.d. realizations $\{\boldsymbol{y}_1, \ldots, \boldsymbol{y}_N\}$ according to

$$p(\boldsymbol{y}|\boldsymbol{X}) = \frac{|\boldsymbol{\Sigma}_{\boldsymbol{X}}|^{-\frac{1}{2}}}{(2\pi)^{T/2}} \exp\left\{-\tfrac{1}{2}\boldsymbol{y}^{\mathsf{T}}\boldsymbol{\Sigma}_{\boldsymbol{X}}^{-1}\boldsymbol{y}\right\}, \tag{90}$$

where $\boldsymbol{\Sigma}_{\boldsymbol{X}} = \boldsymbol{I}_T + \rho\boldsymbol{X}^{\mathsf{T}}\boldsymbol{X}$. Consider the set where $d = \binom{T+1}{2}$ and define

$$\boldsymbol{\Theta} := \left\{\boldsymbol{\theta} \subset \mathbb{R}^d : \tilde{\boldsymbol{\Sigma}}(\boldsymbol{\theta}) \succeq 0\right\} \tag{91}$$

$$I(\boldsymbol{X}; \boldsymbol{Y}) \leq \max_{\boldsymbol{\theta} \in \boldsymbol{\Theta}} I(\boldsymbol{\theta}; \boldsymbol{Y}). \tag{92}$$

Asymptotic Capacity with multivariate Gaussian

The multivariate Gaussian

$$f_{\boldsymbol{\theta}}(\boldsymbol{y}) = \mathcal{N}(0, \boldsymbol{\Sigma}_{\boldsymbol{\theta}}). \tag{93}$$

$$\max_{\boldsymbol{\theta}} I(\boldsymbol{\theta}, \boldsymbol{Y}) = \frac{d}{2}\log\left(\frac{N}{2\pi e}\right) + \log\int_{\boldsymbol{\Theta}} |\boldsymbol{J}(\boldsymbol{\theta})|^{\frac{1}{2}}\, \mathrm{d}\boldsymbol{\theta} + o(1). \tag{94}$$

The Fisher information is given by

$$\boldsymbol{J}_T(\boldsymbol{\theta}) = \mathbb{E}\left[\nabla_{\boldsymbol{\theta}} \ln(f_{\boldsymbol{\theta}}(\boldsymbol{y}))\nabla_{\boldsymbol{\theta}}^{\mathsf{T}} \ln(f_{\boldsymbol{\theta}}(\boldsymbol{y}))\right]. \tag{95}$$

$$[\boldsymbol{J}_T(\boldsymbol{\theta})]_{i,j} = \frac{1}{2}\mathrm{tr}\left\{\boldsymbol{\Sigma}_{\boldsymbol{\theta}}^{-1}\frac{\partial\boldsymbol{\Sigma}_{\boldsymbol{\theta}}}{\partial\theta_i}\boldsymbol{\Sigma}_{\boldsymbol{\theta}}^{-1}\frac{\partial\boldsymbol{\Sigma}_{\boldsymbol{\theta}}}{\partial\theta_j}\right\} \tag{96}$$

need to find

$$c = \int_{\boldsymbol{\theta}} |J(\boldsymbol{\theta})|^{\frac{1}{2}}\, \mathrm{d}\boldsymbol{\theta}. \tag{97}$$

Special case T =1

We have $d = 1$ we have the Fisher information

$$J(\theta) = \frac{\rho^2}{2(1+\rho\theta)^2} \tag{98}$$

with

$$c = \int_0^1 \sqrt{\frac{\rho^2}{2(1+\rho\theta)^2}}\,\mathrm{d}\theta = \frac{1}{\sqrt{2}}\ln(1+\rho). \tag{99}$$

and the asymptotic capacity grows as $N \to \infty$

$$C = \frac{1}{2}\log\left(\frac{N}{4\pi e}\right) + \log\ln(1+\rho), \tag{100}$$

Special case T = 2

$$c = \int_{\boldsymbol{\Theta}} \sqrt{|\boldsymbol{J}_2(\boldsymbol{\theta})|}\, \mathrm{d}\boldsymbol{\theta} \tag{101}$$

where $\boldsymbol{\Theta} = \left\{\boldsymbol{\theta} : \theta_1\theta_3 - \theta_2^2 \geq 0 \text{ and } 0 \leq \theta_1, \theta_3 \leq 1\right\}$ and

$$|\boldsymbol{J}_2(\boldsymbol{\theta})| = \frac{\rho^6}{4\left[(1+\rho\theta_1)(1+\rho\theta_3) - \rho^2\theta_2^2\right]^3} \tag{102}$$

we can retrieve tighter upper and lower bounds on c as explicit functions of ρ

$$\kappa_2^{\mathrm{LB}}(\rho) \leq c \leq \kappa_2^{\mathrm{UB}}(\rho) \tag{103}$$

where

$$\kappa_2^{\mathrm{LB}}(\rho) = \frac{4}{1+\rho} \cdot \left(\rho - \sqrt{\rho(1+\rho)}\sinh^{-1}(\sqrt{\rho})\right) + 8\left(\sinh^{-1}(\sqrt{\rho}) - \sqrt{\frac{\rho}{1+\rho}}\right) \cdot \tanh^{-1}\left(\frac{\sqrt{1+\rho}-1}{\sqrt{\rho}}\right)$$

$$\kappa_2^{\mathrm{UB}}(\rho) = \frac{4}{\sqrt{1+\rho}} \cdot \left(\sqrt{1+\rho}\sinh^{-1}(\sqrt{\rho}) - \sqrt{\rho}\right) \cdot \left(\sqrt{\rho} - \arctan(\sqrt{\rho})\right) \tag{104}$$

Application of Clarke and Barron's Results: Unquantized Non-Coherent Channel (3)

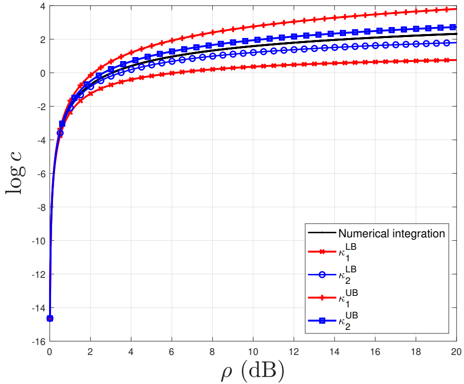

Figure: Normalizing constant as a function of ρ in linear scale along with the updated upper and lower bounds for $T = 2$.

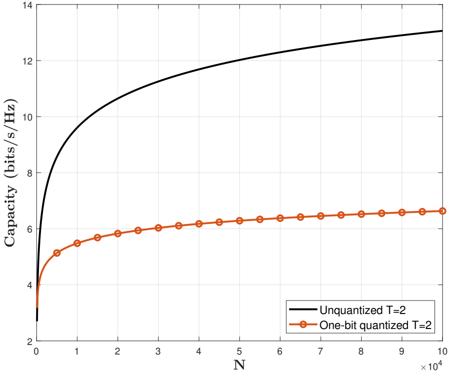

Figure: Comparison between the asymptotic capacity of the unquantized and one-bit quantized channel for $T = 2$ and $\rho = 5$ dB.

Special case $T = 3$

The Fisher information matrix

$$|\boldsymbol{J}_3(\boldsymbol{\theta})|^{\frac{1}{2}} = \frac{\rho^6}{2\sqrt{2}|\boldsymbol{\Sigma}(\boldsymbol{\theta})|^2} \tag{105}$$

Consider the Cholesky parameterization of the covariance matrix $\boldsymbol{\Sigma}(\boldsymbol{\ell}) = \boldsymbol{I}_T + \rho \boldsymbol{L}\boldsymbol{L}^\mathsf{T}$ and $\boldsymbol{\Omega} := \left\{\boldsymbol{\ell} \in \mathbb{R}^d : \boldsymbol{\Sigma}(\boldsymbol{\ell}) \succeq 0\right\}$. The Fisher matrix is covariant under parameterization as

$$\boldsymbol{J}(\boldsymbol{\ell}) = \left[\frac{\partial \boldsymbol{\theta}}{\partial \boldsymbol{\ell}}\right]^\mathsf{T} \boldsymbol{J}(\boldsymbol{\theta}(\boldsymbol{\ell})) \left[\frac{\partial \boldsymbol{\theta}}{\partial \boldsymbol{\ell}}\right] \tag{106}$$

the Fisher matrix determinant can be re-written as

$$|\boldsymbol{J}(\boldsymbol{\ell})|^{\frac{1}{2}} = |\boldsymbol{J}(\boldsymbol{\theta}(\boldsymbol{\ell}))|^{\frac{1}{2}} . \left|\frac{\partial \boldsymbol{\theta}}{\partial \boldsymbol{\ell}}\right| = \frac{\rho^6}{2\sqrt{2}|\boldsymbol{\Sigma}(\boldsymbol{\ell})|^2} \cdot 8\ell_1^3 \ell_3^2 \ell_6, \tag{107}$$

Application of Clarke and Barron's Results: Unquantized Non-Coherent Channel (3)

U

sing the following identity:

$$|\boldsymbol{A}| \leq \exp\{\operatorname{tr}\{\boldsymbol{A} - \boldsymbol{I}\}\} \ \text{ and } \ |\boldsymbol{\Sigma}(\boldsymbol{\ell})| \leq \exp\left\{\rho \sum_{i=1}^{6} \ell_i^2\right\} \tag{108}$$

the lower bound is

$$c \geq 2\sqrt{2}\rho^6 \int_{\boldsymbol{\Omega}} \ell_1^3 \ell_3^2 \ell_6 \exp\left\{-2\rho \sum_{i=1}^{6} \ell_i^2\right\} \mathrm{d}\boldsymbol{\ell} = \frac{\pi^2}{256\sqrt{2}} \cdot \frac{(e^{2\rho} - 2\rho - 1)^3}{e^{6\rho}}. \tag{109}$$

For general $T > 3$

For general $T > 3$, we can follow the same approach

$$\begin{aligned} \int_{\boldsymbol{\Theta}} |\boldsymbol{J}(\boldsymbol{\theta})|^{\frac{1}{2}} \, \mathrm{d}\boldsymbol{\theta} &= \int_{\boldsymbol{\Omega}} |\boldsymbol{J}_T(\boldsymbol{\theta}(\boldsymbol{\ell}))|^{\frac{1}{2}} \cdot \left|\frac{\partial \boldsymbol{\theta}}{\partial \boldsymbol{\ell}}\right| \mathrm{d}\boldsymbol{\ell} \\ &= 2^T \int_{\boldsymbol{\Omega}} \prod_{i=1}^{T} (1 + \rho \ell_{ii}^2)^{-(T+1)} (\ell_{ii})^{T-i+1} \, \mathrm{d}\boldsymbol{\ell} \end{aligned} \tag{110}$$